The atypical cation-conduction and gating properties of ELIC underscore the marked functional versatility of the pentameric ligand-gated ion-channel fold

Giovanni Gonzalez-Gutierrez[1] and Claudio Grosman[1,2,3]

[1]Department of Molecular and Integrative Physiology, [2]Center for Biophysics and Computational Biology, and [3]Neuroscience Program, University of Illinois at Urbana-Champaign, Urbana, IL 61801

The superfamily of pentameric ligand-gated ion channels (pLGICs) is unique among ionotropic receptors in that the same overall structure has evolved to generate multiple members with different combinations of agonist specificities and permeant-ion charge selectivities. However, aside from these differences, pLGICs have been typically regarded as having several invariant functional properties. These include pore blockade by extracellular quaternary-ammonium cations in the micromolar-to-millimolar concentration range (in the case of the cation-selective members), and a gain-of-function phenotype, which manifests as a slower deactivation time course, as a result of mutations that reduce the hydrophobicity of the transmembrane pore lining. Here, we tested this notion on three distantly related cation-selective members of the pLGIC superfamily: the mouse muscle nicotinic acetylcholine receptor (nAChR), and the bacterial GLIC and ELIC channels. Remarkably, we found that, whereas low millimolar concentrations of TMA^+ and TEA^+ block the nAChR and GLIC, neither of these two quaternary-ammonium cations blocks ELIC at such concentrations; instead, both carry measurable inward currents when present as the only cations on the extracellular side. Also, we found that, whereas lidocaine binding speeds up the current-decay time courses of the nAChR and GLIC in the presence of saturating concentrations of agonists, the binding of lidocaine to ELIC slows this time course down. Furthermore, whereas mutations that reduce the hydrophobicity of the side chains at position 9′ of the M2 α-helices greatly slowed the deactivation time course of the nAChR and GLIC, these mutations had little effect—or even sped up deactivation—when engineered in ELIC. Our data indicate that caution should be exercised when generalizing results obtained with ELIC to the rest of the pLGICs, but more intriguingly, they hint at the possibility that ELIC is a representative of a novel branch of the superfamily with markedly divergent pore properties despite a well-conserved three-dimensional architecture.

INTRODUCTION

Structure–function studies of bacterial pentameric ligand-gated ion channels (pLGICs) have led to the notion that both structure and function are remarkably well-conserved in the superfamily despite little amino acid sequence conservation. Indeed, even in the absence of the eponymous cysteine loop or the long intracellular linker between the M3 and M4 transmembrane α-helices, the bacterial members studied thus far open and desensitize upon binding extracellular ligands, much like their homologues from the nervous system of animals (Bocquet et al., 2007; Gonzalez-Gutierrez and Grosman, 2010; Parikh et al., 2011; Zimmermann and Dutzler, 2011; Gonzalez-Gutierrez et al., 2012).

From studies performed largely on the animal members of the superfamily, it has been concluded that—aside from being activated by different ligands and having opposite charge selectivities—pLGICs form a group of ion channels that share several functional properties. For example: (a) the transmembrane pore of the cation-selective members is blocked by extracellular quaternary-ammonium cations in the micromolar-to-millimolar concentration range (Neher and Steinbach, 1978; Adler et al., 1979; Sine and Steinbach, 1984; Ogden and Colquhoun, 1985; Marshall et al., 1990; Cuevas and Adams, 1994; Zhang et al., 1995; Blanchet and Dulon, 2001; Akk and Steinbach, 2003; Purohit and Grosman, 2006), discriminates poorly among monovalent cations (Adams et al., 1980; Yang, 1990), and displays some permeability to Ca^{2+} (Adams et al., 1980; Decker and Dani, 1990; Yang 1990; Zhou and Neher, 1993; Elenes et al., 2009); (b) the transmembrane pore of the anion-selective members is blocked by picrotoxin (Chang and Weiss, 1998, 1999; Etter et al., 1999; Sedelnikova et al., 2006; Bali and Akabas, 2007; Wang et al., 2007); (c) the rearrangement of the loop between the extracellular domain β-strands 9 and 10 (the C-loop) is an integral part of the

Correspondence to Claudio Grosman: grosman@illinois.edu

Abbreviations used in this paper: ACh, acetylcholine; ELIC, ligand-gated ion channel from *Erwinia chrysanthemi*; GLIC, ligand-gated ion channel from *Gloeobacter violaceus*; nAChR, nicotinic acetylcholine receptor; pLGIC, pentameric ligand-gated ion channel; TMA^+, tetramethylammonium; TPA^+, tetrapropylammonium.

The Rockefeller University Press $30.00
J. Gen. Physiol. Vol. 146 No. 1 15–36
www.jgp.org/cgi/doi/10.1085/jgp.201411333

conformational changes that occur upon ligand binding or gating (Chen et al., 1995; Hansen et al., 2005; Mukhtasimova et al., 2009; Hibbs and Gouaux, 2011; Purohit and Auerbach, 2013; Yoluk et al., 2013); and (d) mutations that reduce the hydrophobicity of the transmembrane pore lining invariably lead to a gain-of-function phenotype (regardless of the channel's charge selectivity) that results from a stabilized open-channel conformation and manifests, for example, as an increased sensitivity to agonists, an increased unliganded-gating activity, longer bursts and clusters of single-channel openings, a slower time course of deactivation, and a slower time course of desensitization (Revah et al., 1991; Filatov and White, 1995; Labarca et al., 1995; Kearney et al., 1996; Chang and Weiss, 1998, 1999; Thompson et al., 1999; Kosolapov et al., 2000; Bianchi and Macdonald, 2001; Cymes et al., 2002; Burzomato et al., 2003; Grosman, 2003; Shan et al., 2003; Cymes et al., 2005; Papke and Grosman, 2014). Importantly, the discovery of the more distantly related bacterial and archaeal pLGICs (Tasneem et al., 2005) has afforded us the possibility to challenge these concepts in the framework of an even more diverse group of homologues. Although it seems likely that all members of the superfamily—from bacterial and archaeal to human—form ion channels gated by extracellular ligands, the degree to which more detailed aspects of molecular function are conserved remains to be ascertained.

Not much is known about the relationship between structure and function in bacterial or archaeal pLGICs, but some intriguing differences have already begun to emerge. A case in point is the C-loop of the extracellular domain. Whereas mutations to this loop have been found to impair the activation of animal pLGICs profoundly (Chen et al., 1995; Shen et al., 2012), we have recently shown that the entire C-loop of the bacterial homologue ligand-gated ion channel from *Gloeobacter violaceus* (GLIC) can be deleted without compromising its function as a proton-gated channel (Gonzalez-Gutierrez et al., 2013). Another example is the atypical phenotype of leucine-to-alanine mutations at the pore-lining position 9′ of the M2 transmembrane α-helix of ligand-gated ion channel from *Erwinia chrysanthemi* (ELIC; Gonzalez-Gutierrez et al., 2012), a finding that we investigate further here with additional mutations. Yet another example is the larger number of exponential components observed for the distribution of open times of ELIC recorded at saturating concentrations of agonist (propylamine) compared with the single component observed under comparable experimental conditions in the cases of the (animal) muscle nicotinic acetylcholine receptor (nAChR) and the α1 glycine receptor (Marabelli et al., 2015).

In this paper, we set out to study some of the properties of the transmembrane pore. We compared the effects of pore blockers (tetramethylammonium [TMA^+], tetraethylammonium [TEA^+], and lidocaine) and mutations to the pore's hydrophobic lining on the function of three distantly related cation-selective members of the superfamily: the mouse muscle nAChR, and the bacterial GLIC and ELIC channels. Strikingly, we found that, whereas millimolar concentrations of extracellular TMA^+ and TEA^+ block the nAChR and GLIC, neither of these two quaternary-ammonium cations blocks ELIC at a concentration as high as 50 mM, and instead, both carry measurable inward currents when present as the only cations on the extracellular side. Also, we found that, whereas lidocaine binding speeds up the time course of the current decay of the nAChR and GLIC on sustained application of saturating concentrations of agonist, the binding of lidocaine to ELIC slows this time course down, and the crystal structure of the ELIC–lidocaine complex shows the anesthetic bound to the cavity lined by the back of the M2 and the front of the M1 and M3 transmembrane α-helices. In marked contrast, in both the nAChR (Leonard et al., 1988; Charnet et al., 1990) and GLIC (Hilf et al., 2010), lidocaine (or its trimethyl-ammonium counterpart, QX-222) has been found to bind to the transmembrane pore, i.e., the cavity lined by the front side of the five M2 α-helices. Finally, whereas mutations that reduce the hydrophobicity of the pore-lining side chains greatly slowed down the time course of deactivation of the nAChR and GLIC—a phenomenon often regarded as a hallmark of the entire superfamily—we found that these mutations have little or even the opposite effect when engineered in ELIC.

MATERIALS AND METHODS

cDNA clones, mutagenesis, and heterologous expression

HEK-293 cells were transiently transfected with wild-type or mutant complementary DNAs (cDNAs) coding the mouse muscle adult-type nAChR (α1, β1, δ, and ε subunits), GLIC or ELIC using the calcium-phosphate precipitation method. nAChR cDNAs in the expression vector pRBG4 were provided by S. Sine (Mayo Clinic, Rochester, MN). GLIC and ELIC cDNAs in the pcDNA 3.1 (−) vector (Life Technologies) were prepared as described previously (Gonzalez-Gutierrez and Grosman, 2010; Gonzalez-Gutierrez et al., 2012). For the calculation of identities and similarities between pairs of amino acid sequences, the number of identical or similar residues was divided by the average number of total residues in the two aligned sequences. Point mutations were engineered using the QuikChange site-directed mutagenesis kit (Agilent Technologies) and were confirmed by dideoxy sequencing.

Electrophysiological recordings and analysis

Ensemble (macroscopic) currents were recorded from transfected HEK-293 cells using the outside-out configuration of the patch-clamp technique, whereas single-channel currents were recorded using either the outside-out or the cell-attached configuration, at ∼22°C. For outside-out recordings, the ligand was applied to the external aspect of excised patches as rapid jumps (solution-exchange $time_{10–90\%} < 150$ µs). These step-changes in the concentration of ligand were achieved by the rapid switching of two solutions flowing from either barrel of a piece of theta-type

capillary glass mounted on a piezo-electric device (Burleigh-LSS-3100; discontinued). For all outside-out recordings, the patch-pipette solution consisted of (in mM) 110 KF, 40 KCl, 1 $CaCl_2$, 11 EGTA, and 10 HEPES/KOH, pH 7.4; the solutions flowing through the two barrels of the perfusion tubing differed among experiments and are indicated in the text. For cell-attached recordings, the pipette solution consisted of (in mM) 142 KCl, 5.4 NaCl, 1.8 $CaCl_2$, 1.7 $MgCl_2$, 10 HEPES/KOH, pH 7.4, and the indicated agonist. The effective bandwidth for data analysis was DC–5 kHz for both macroscopic and single-channel currents. For display purposes, the macroscopic current traces were decimated, and the single-channel traces were filtered such that the cut-off frequency was 2–5 kHz. Both macroscopic and single-channel current recordings were analyzed using pClamp 9.0 (MDS Analytical Technologies).

To determine the effects of quaternary-ammonium cations and lidocaine on the values of macroscopic peak currents and decay time constants of the muscle nAChR and GLIC, we used paired experiments. In these, the response of each patch of membrane to a pulse of agonist was recorded sequentially in the absence, in the presence, and back again in the absence (that is, upon washout) of the compound under study with the goal of reducing the impact of the variability from patch to patch. Thus, each patch acted as its own control and generated a value for the effect of each added compound. These values (obtained from several patches) were averaged, and the corresponding mean and standard error are presented in the form of bar graphs throughout the paper as normalized peak currents and normalized time constants. In the case of ELIC, however, paired experiments proved difficult because the channel activity usually ran down as a function of time after patch excision. Therefore, to maximize the amount of data obtained from each patch, the number of maneuvers within each single experiment was kept to a minimum. Thus, responses in the presence and in the absence of the tested compounds were recorded from separate (i.e., unpaired) patches of membrane. The ratios between the means of these values were calculated, and their corresponding standard errors were propagated; it is these values of ELIC that are presented in the form of bar graphs throughout the paper.

Because of the slow desensitization time courses of wild-type GLIC and ELIC (with time constants, in some patches, as slow as 8 s), the agonist typically had to be applied for long intervals (~1 min) for the currents to reach steady state, and hence, for accurate estimates of the exponential decay time constants to be obtained. These intervals proved to be too long, however, considering the average lifetime of a fast-perfused outside-out patch, on the one hand, and the multiple solution changes and consecutive agonist applications that we intended to perform on any given patch, on the other. Therefore, as a compromise, we applied 1-min pulses of agonist to only a few patches per tested condition and estimated the steady-state value of the current relative to the peak. With this information, we then proceeded to fix the steady-state current of fits to responses to shorter applications of agonist (5 s). In all cases, the steady-state values of the macroscopic currents on sustained application of agonist turned out to be nearly zero.

In an attempt to assess the statistical significance of the differences between the mean values of current decay time constants obtained under different conditions, we performed Student's *t* tests (paired or unpaired, depending on the experimental design) and report the corresponding two-tailed p-values.

Protein purification, crystallization, and x-ray diffraction

ELIC was purified as described in previous work (Gonzalez-Gutierrez et al., 2012). Concentrated protein (~10 mg/ml) was mixed with cysteamine (final concentration = 10 mM), *Escherichia coli* total polar lipids (Avanti Polar; final concentration = 0.5 mg/ml), and lidocaine (final concentration = 15 mM) or the bromo derivative *N*-1-(4-bromophenyl)-*N*-2,*N*-2 diethyl glycinamide (Chembridge; final concentration = 15 mM). The protein was crystallized by vapor diffusion in hanging drops at 4°C. The reservoir solution consisted of 200 mM $(NH_4)_2SO_4$, 10–12% (wt/vol) PEG 4000 and 50 mM N-(2-acetamido) iminodiacetic acid/NaOH, pH 6.5–6.7. For cryoprotection, crystals were transferred for a few seconds into reservoir solution supplemented with 30% (vol/vol) ethylene-glycol and were subsequently flash frozen in liquid nitrogen. Diffraction data were collected at 100 K at the 21 ID–D/F/G beamline at the Advanced Photon Source (Argonne National Laboratory, Argonne, IL). The data were indexed, integrated, and scaled using HKL2000 (Otwinowski and Minor, 1997). The structures were solved by molecular replacement using PDB deposition 2VL0 as the search model. The Auto Build function in PHENIX (Adams et al., 2010) was used to generate a first model that was subsequently refined in PHENIX and Coot (Emsley et al., 2010). No attempts were made to refine regions of poor electron density as defined in the starting model. Cross-validation used 5% of the data in the calculation of the R_{free} value. PyMOL was used to prepare molecular images (The PyMOL Molecular Graphics System, Version 1.3; Schrödinger). The structure of ELIC was solved in the presence of cysteamine and lidocaine to a resolution of 3.65 Å; the wavelength used was 0.97872 Å. Because only a weak density for lidocaine was observed, a second structure in the presence of cysteamine and the bromo derivative *N*-1-(4-bromophenyl)-*N*-2,*N*-2 diethyl glycinamide was also solved (to a resolution of 4.23 Å). To confirm the presence of the heavy atom, a third dataset was obtained using a wavelength of 0.91838 Å (solved to a resolution of 4.82 Å).

RESULTS

Effects of quaternary-ammonium cations and lidocaine on the nAChR and GLIC

To gain insight into the extent to which concepts derived from the study of the bacterial homologues of the pLGIC superfamily can be applied to their animal counterparts, we decided to compare some of their functional properties. We started by testing the effects of TEA^+ and lidocaine on the (heteromeric) adult-type nAChR from mouse muscle, and the (homomeric) GLIC and ELIC channels from bacteria. Averaging the four types of subunit, the amino acid sequence of this nAChR is 16.7% identical (25.4% similar) to that of GLIC and 14.7% identical (23.1% similar) to that of ELIC. The amino acid sequence of GLIC is 20.4% identical (35.2% similar) to that of ELIC. Disregarding the highly variable M3–M4 linker, these values become 19.0% (identity) and 33.0% (similarity) for the muscle AChR and GLIC; 16.9% (identity) and 30.4% (similarity) for the muscle AChR and ELIC; and 20.5% (identity) and 35.8% (similarity) for GLIC and ELIC.

TEA^+ applied to the extracellular side of outside-out patches at a concentration of 0.5–5.0 mM reduced the peak amplitude of the macroscopic currents flowing through the nAChR and GLIC with little (if any) effect on their time constants of desensitization (Figs. 1 and 2, and Table 1). The lower peak values of the nAChR-mediated macroscopic currents can be attributed to a

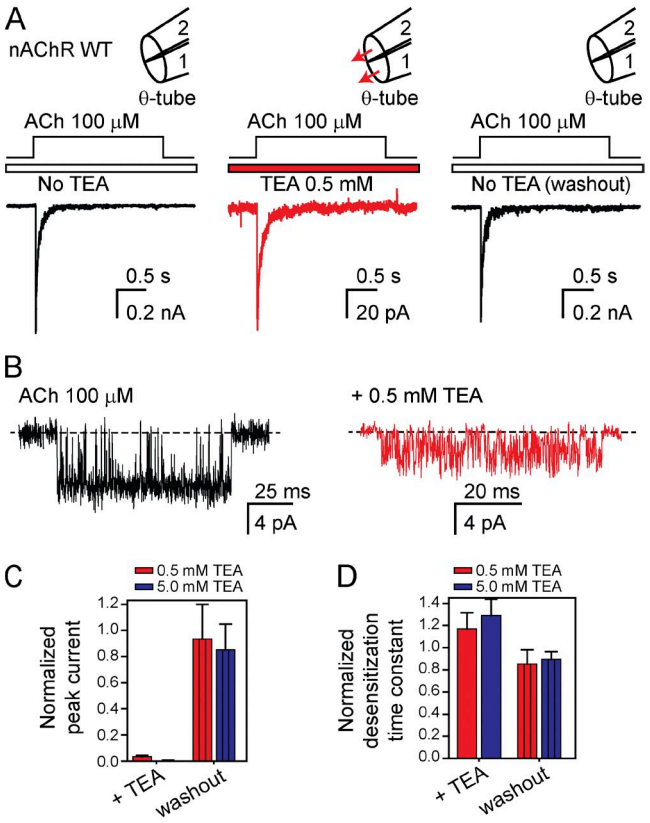

Figure 1. Block of the muscle nAChR by TEA^+. (A) Macroscopic current responses to 2-s pulses of 100 μM ACh recorded at –80 mV from the mouse muscle adult-type nAChR in the outside-out configuration. The response of each patch of membrane was recorded sequentially in the absence of TEA^+ (left), in the presence of 0.5 mM TEA^+ flowing through both barrels of the theta-type perfusion tubing (middle), and back again, without TEA^+ in either barrel (right). The solutions flowing through the two barrels of the perfusion tubing were (in mM) 142 KCl, 5.4 NaCl, 1.8 $CaCl_2$, 1.7 $MgCl_2$, and 10 HEPES/KOH, pH 7.4 with or without ACh and with or without TEA^+. In the schematic representations of the theta-tubing perfusion, arrows indicate the application of TEA^+. Note the expanded current scale used for the middle panel; the trace is the average of 25 consecutive responses recorded from a representative patch. (B) Single-channel inward currents elicited by 100 μM ACh recorded in the presence or absence of 0.5 mM TEA^+ at approximately –80 mV in the cell-attached configuration; openings are downward deflections. The pipette solution was (in mM) 142 KCl, 5.4 NaCl, 1.8 $CaCl_2$, 1.7 $MgCl_2$, 0.1 ACh, and 10 HEPES/KOH, pH 7.4 with or without TEA^+. (C) Peak-current amplitudes recorded in response to the application of ACh in the presence of external 0.5 mM or 5.0 mM TEA^+ and upon TEA^+ removal normalized to the peak value observed in the initial TEA^+-free recording. (D) Time constant of desensitization during the application of ACh in the presence of external 0.5 or 5.0 mM TEA^+ and upon TEA^+ removal normalized to the time constant fitted to the initial TEA^+-free recording. The values plotted in C and D are means obtained from six patches each for the two concentrations of TEA^+; error bars are the corresponding standard errors.

combination of a decreased single-channel conductance and a lower open probability (Fig. 1 B), consistent with TEA^+ acting as a pore blocker that enters and exits the pore fast enough to reduce the unitary current

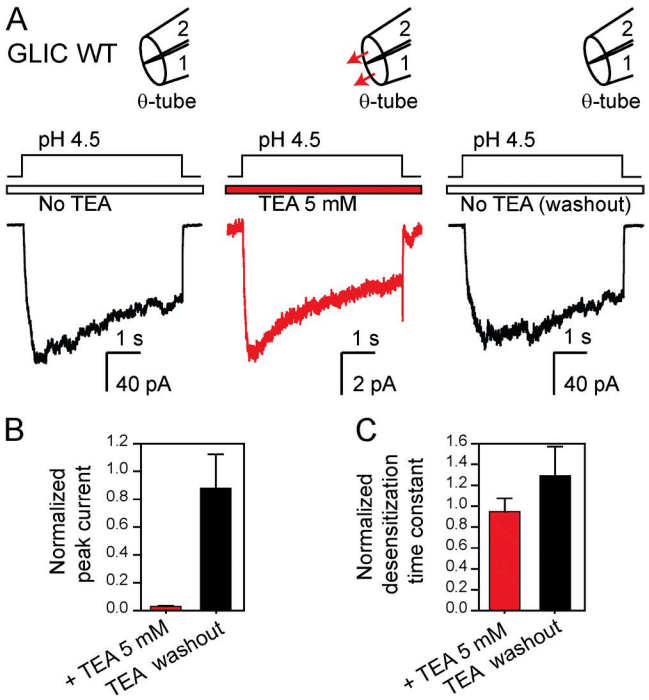

Figure 2. Block of GLIC by TEA^+. (A) Macroscopic current responses to 5-s pulses of pH 4.5 solution ($pH_{holding}$ 7.4) recorded at –80 mV in the outside-out configuration. The response of each patch of membrane was recorded sequentially in the absence of TEA^+ (left), in the presence of 5 mM TEA^+ flowing through both barrels of the theta-type perfusion tubing (middle), and back again, without TEA^+ in either barrel (right). The solutions flowing through the two barrels of the perfusion tubing were (in mM) 142 KCl, 5.4 NaCl, 1.8 $CaCl_2$, 1.7 $MgCl_2$ with or without TEA^+, and pH buffered with 10 mM HEPES/KOH, pH 7.4, or with 10 mM acetic acid/KOH, pH 4.5. In the schematic representations of the theta-tubing perfusion, arrows indicate the application of TEA^+. Note the expanded current scale used for the middle panel; the trace is the average of 25 consecutive responses recorded from a representative patch. (B) Peak-current amplitudes recorded in response to the application of pH 4.5 in the presence of external 5 mM TEA^+ and upon TEA^+ removal normalized to the peak value observed in the initial TEA^+-free recording. (C) Time constants of desensitization during the application of pH 4.5 in the presence of external 5 mM TEA^+ and upon TEA^+ removal normalized to the time constant fitted to the initial TEA^+-free recording. The values plotted in B and C are means obtained from 6 patches; error bars are the corresponding standard errors.

amplitude yet slow enough for the individual blocking events to be discernible as sojourns in the zero-current level. Although analogous recordings from GLIC were not clear enough to draw meaningful conclusions (owing to the low single-channel conductance of this bacterial channel even in the absence of TEA^+), we surmise that the effect of this organic cation on GLIC is essentially the same. Regarding desensitization of these two channels, we would like to highlight the observation that the presence of blocking concentrations of TEA^+ did not affect their time courses. Thus, the presence of a blocker inside the pore of a pLGIC's crystal structure, for example, should not be taken to imply

TABLE 1

Effect of quaternary-ammonium cations and lidocaine on the time course of current decay upon sustained exposure to agonist

Channel	Conditions	τ_{decay}		P-value	Number of patches
		(mean ± SE; ms)	(range; ms)		
Wild-type nAChR	Control	37.0 ± 8.8	16.7–63.7	0.37	6
	0.5 mM TEA^+	41.2 ± 10.5	23.9–74.6		
Wild-type nAChR	Control	48.9 ± 6.8	22.8–61.9	0.11	6
	5 mM TEA^+	59.5 ± 5.5	42.3–73.8		
Wild-type nAChR	Control	59.8 ± 3.7	51.9–67.1	7.6×10^{-7}	4
	0.5 mM lidocaine	0.60 ± 0.07	0.45–0.71		
Wild-type GLIC	Control	2,197 ± 950	154–3,928	0.34	6
	5 mM TEA^+	1,749 ± 737	146–4,057		
Wild-type GLIC	Control	2,072 ± 452	195–5,360	4.3×10^{-3}	12
	0.5 mM lidocaine	698 ± 208	36.7–2,045		
Wild-type ELIC	Control	4,533 ± 584	2,397–8,026	–	9
	50 mM TEA^+	5,353 ± 988	2,443–10,324	0.22	8
	5 mM TEA^+ (pipette)	5,370 ± 531	3,979–6,677	0.16	5
	5 mM lidocaine	unmeasurably slow	–	–	14
	50 mM TMA^+	4,726 ± 782	1,608–7,725	0.84	9
L9′A + F16′L ELIC	Control	unmeasurably slow	–	–	17
	50 mM TEA^+	unmeasurably slow	–	–	7
	50 mM TMA^+	unmeasurably slow	–	–	11

that the crystallized conformation represents the open state because pore block (at least by TEA^+) does not prevent channel desensitization.

Extracellular lidocaine also reduced the peak currents mediated by the nAChR (Fig. 3, A and B), but unlike TEA^+, this local anesthetic sped up the time course of current decay by a factor of ∼100 (Fig. 3 C and Table 1). The lower peak values of the nAChR-mediated macroscopic currents can be attributed to the dramatically reduced single-channel open probability elicited by 100-µM ACh in the presence of 0.5 mM lidocaine (Fig. 3 A, insets). Because lidocaine is a slower blocker of the nAChR than is TEA^+ (note that, in the presence of lidocaine, the amplitude of the single-channel currents remained essentially unaltered), it may be asked whether the faster decay of the macroscopic currents reflects faster desensitization or merely the kinetics of lidocaine entry into the open-channel pore. To learn more about the effect of lidocaine, we coapplied it with ACh for short intervals (Fig. 3 D). If lidocaine acted as a fast-dissociating open-channel blocker that does not alter the kinetics of closed–open–desensitized state interconversions, for example, the current upon washout of both lidocaine and ACh would be expected to rebound and attain the same value as that observed at the end of ACh-only pulses. This is not what we observed, however. Upon lidocaine and ACh washout, the signal remained close to the zero-current baseline (Fig. 3 D, vertical dashed line), a finding that is entirely consistent with lidocaine strongly biasing the channel's conformational landscape toward a nonconductive conformation (such as the desensitized state). However, it may be argued that this finding is also consistent with lidocaine dissociating slowly from the open-channel pore. As a result, we do not refer to this particular current decay time course as the time course of desensitization. Clearly, more experiments would be needed to elucidate the relative contributions of pore block and entry into desensitization to the current decay time course of the nAChR in the presence of both ACh and lidocaine. Obtaining such mechanistic insight was beyond the scope of this paper, however.

In the case of GLIC, the effect of extracellular 0.5 mM lidocaine on the macroscopic currents was qualitatively the same as that on the nAChR. Indeed, the peak currents were decreased to a large extent (Fig. 4, A and B), and the current-decay time course on continuous exposure to pH 4.5 extracellular solution was sped up, although in this case, only by a factor of ∼3 (Fig. 4 C and Table 1). In fact, the ranges of time constant values of GLIC with and without lidocaine overlapped partially (Table I), but the application of lidocaine to each individual patch (as illustrated in Fig. 4 A) sped up the time course of current decay in all 12 tested patches. The time constant fitted to each patch varied widely from patch to patch, but its value always became faster upon adding lidocaine (and thus, we cannot explain the slowing effect reported by Velisetty and Chakrapani (2012) for lidocaine on the current-decay time course of GLIC). Again, although single-channel recordings from GLIC in the presence of lidocaine were not clear enough to draw conclusions, it seems likely that this local anesthetic also lowers the channel's open probability, much like it does on the nAChR.

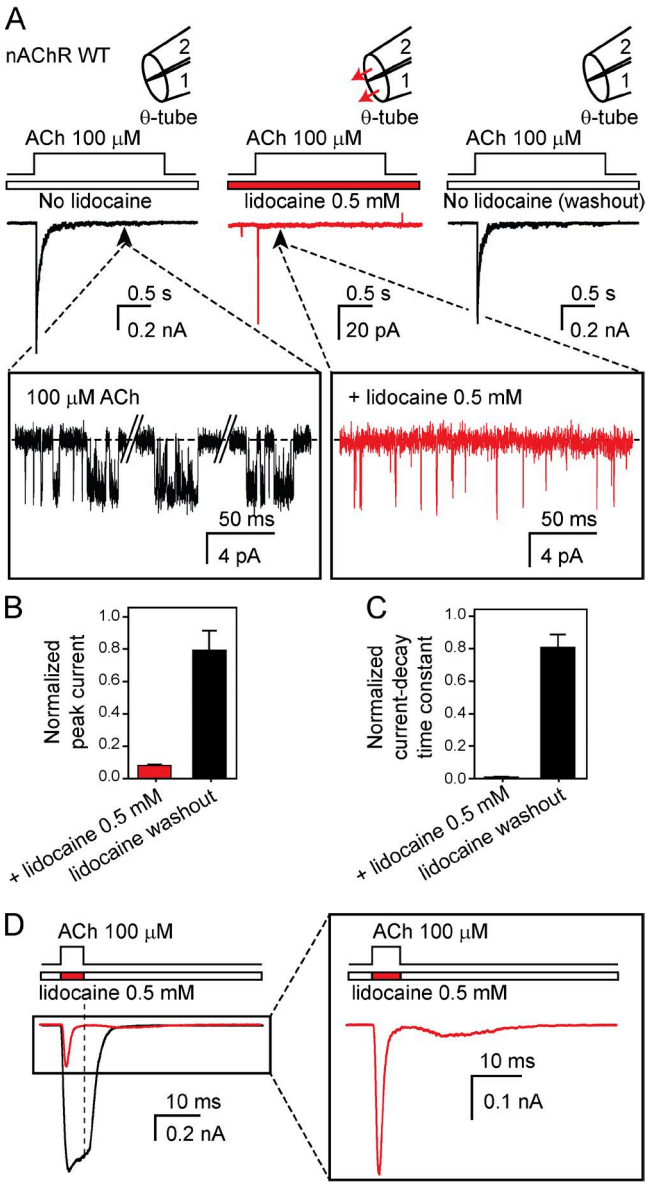

Figure 3. Block of the muscle nAChR by lidocaine. (A) Macroscopic current responses to 2-s pulses of 100 μM ACh recorded at –80 mV from the mouse muscle adult-type nAChR in the outside-out configuration. The response of each patch of membrane was recorded sequentially in the absence of lidocaine (left), in the presence of 0.5 mM lidocaine flowing through both barrels of the theta-type perfusion tubing (middle), and back again, without lidocaine in either barrel (right). The insets show the much lower open probability of the channel in the presence of 0.5 mM external lidocaine; openings are downward deflections. The solutions flowing through the two barrels of the perfusion tubing were (in mM) 142 KCl, 5.4 NaCl, 1.8 $CaCl_2$, 1.7 $MgCl_2$, and 10 HEPES/KOH, pH 7.4 with or without ACh and with or without lidocaine. In the schematic representations of the theta-tubing perfusion, arrows indicate the application of lidocaine. Note the expanded current scale used for the middle panel; the trace is the average of 25 consecutive responses recorded from a representative patch. (B) Peak-current amplitudes recorded in response to the application of ACh in the presence of external 0.5 mM lidocaine and upon lidocaine removal normalized to the peak value observed in the initial lidocaine-free recording. (C) Current-decay time constants during the application of ACh in the presence of external 0.5 mM lidocaine and upon lidocaine removal normalized to the time constant fitted to the initial lidocaine-free recording. The values plotted in B and C are means obtained from 4 patches; error bars are the corresponding standard errors. (D) Comparison of the responses of the nAChR to 5-ms pulses of ACh alone and ACh plus lidocaine applied sequentially to the same patch of membrane. The vertical dashed line emphasizes the different current values observed upon fast washout.

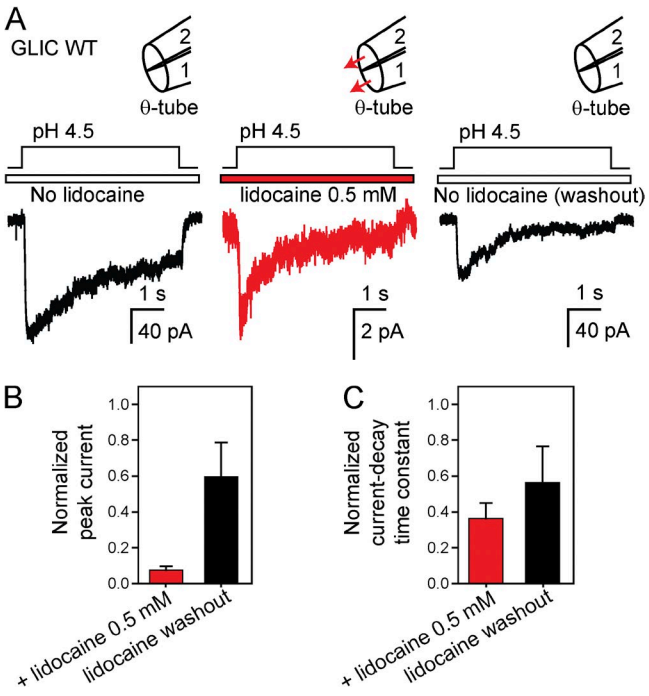

Figure 4. Block of GLIC by lidocaine. (A) Macroscopic current responses to 5-s pulses of pH-4.5 solution ($pH_{holding}$ 7.4) recorded at –80 mV in the outside-out configuration. The response of each patch of membrane was recorded sequentially in the absence of lidocaine (left), in the presence of 0.5 mM lidocaine flowing through both barrels of the theta-type perfusion tubing (middle), and back again, without lidocaine in either barrel (right). The solutions flowing through the two barrels of the perfusion tubing were (in mM) 142 KCl, 5.4 NaCl, 1.8 $CaCl_2$, 1.7 $MgCl_2$ with or without lidocaine, and pH-buffered with 10 mM HEPES/KOH, pH 7.4, or with 10 mM acetic-acid/KOH, pH 4.5. In the schematic representations of the theta-tubing perfusion, arrows indicate the application of lidocaine. Note the expanded current scale used for the middle panel; the trace is the average of 25 consecutive responses recorded from a representative patch. (B) Peak-current amplitudes recorded in response to the application of pH 4.5 in the presence of external 0.5 mM lidocaine and upon lidocaine removal normalized to the peak value observed in the initial lidocaine-free recording. (C) Current-decay time constants during the application of pH 4.5 in the presence of external 0.5 mM lidocaine and upon lidocaine removal normalized to the time constant fitted to the initial lidocaine-free recording. The values plotted in B and C are means obtained from 12 patches; error bars are the corresponding standard errors.

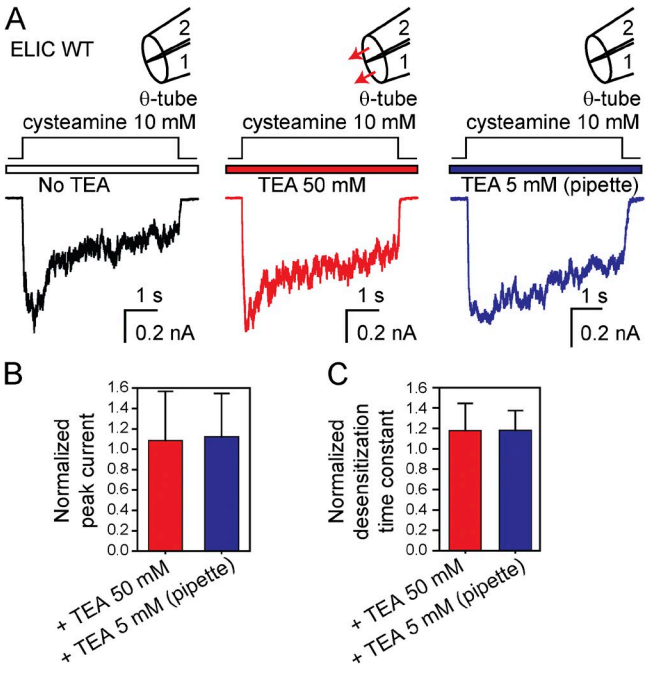

Figure 5. 50 mM TEA^+ fails to block ELIC. (A) Macroscopic current responses to 5-s pulses of 10 mM cysteamine recorded at –80 mV in the outside-out configuration. The responses were recorded without TEA^+ in either barrel (left) or in the presence of 50 mM TEA^+ flowing through both barrels of the theta-type perfusion tubing (middle). Because ELIC displayed marked rundown in outside-out patches, these traces were not recorded sequentially. Instead, individual patches of membrane were exposed to cysteamine pulses either in the absence or the presence of TEA^+. In separate recordings, TEA^+ was also applied to the intracellular side of outside-out patches (right). The solutions flowing through the two barrels of the perfusion tubing were (in mM) 142 KCl, 5.4 NaCl, 1.8 $CaCl_2$, 1.7 $MgCl_2$, and 10 HEPES/KOH, pH 7.4 with or without cysteamine and with or without TEA^+. In the schematic representations of the theta-tubing perfusion, arrows indicate the application of external TEA^+. (B) Peak-current amplitudes recorded in response to the application of cysteamine in the presence of external 50 mM TEA^+ or internal 5 mM TEA^+ normalized to the peak value observed in the absence of external or internal TEA^+. (C) Time constants of desensitization during the application of cysteamine in the presence of external 50 mM TEA^+ or internal 5 mM TEA^+ normalized to the time constant fitted to TEA^+-free recordings. The values plotted in B and C are means obtained from 8 (external 50 mM TEA^+) and 5 (internal 5 mM TEA^+) patches; error bars are the corresponding standard errors. Note the lack of effect of millimolar TEA^+ applied to either side of the membrane.

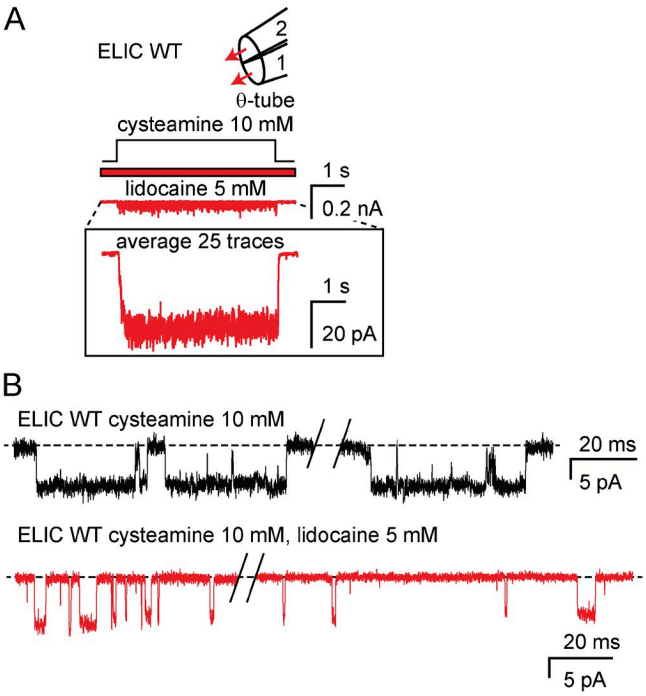

Figure 6. Lidocaine effects on ELIC. (A) Macroscopic current response to 5-s pulses of 10 mM cysteamine in the continuous presence of 5 mM lidocaine recorded at –80 mV in the outside-out configuration. The trace shown is the average of 25 consecutive responses recorded from a representative patch. The solutions flowing through the two barrels of the perfusion tubing were (in mM) 142 KCl, 5.4 NaCl, 1.8 $CaCl_2$, 1.7 $MgCl_2$, 5 lidocaine, and 10 HEPES/KOH, pH 7.4 with or without cysteamine. In the schematic representation of the theta-tubing perfusion, arrows indicate the application of lidocaine. (B) Single-channel inward currents elicited by 10 mM cysteamine recorded at –80 mV in the absence (top) or presence (bottom) of 5 mM lidocaine in the outside-out configuration; openings are downward deflections. The external solution was (in mM) 142 KCl, 5.4 NaCl, 1.8 $CaCl_2$, 1.7 $MgCl_2$, 10 cysteamine, and 10 HEPES/KOH, pH 7.4, with or without lidocaine.

Effects of quaternary-ammonium cations and lidocaine on ELIC

When tested on ELIC, extracellular TEA^+ did not block the peak-current values elicited by saturating (10 mM) cysteamine, even when applied at a concentration as high as 50 mM (Fig. 5, A and B); neither did TEA^+ block the channel when applied to the intracellular side of outside-out patches at a concentration of 5 mM (Fig. 5, A and B). Not surprisingly then, we found that ELIC's kinetics of desensitization are essentially unaffected by the presence of TEA^+ on either side of the membrane (Fig. 5 C and Table 1). Importantly, ELIC's open probability between desensitized intervals in the presence of 10 mM cysteamine and the absence of TEA^+ is similar (∼0.95; Gonzalez-Gutierrez et al., 2012) to that of the muscle nAChR in the presence of 100-µM ACh and the absence of TEA^+ (∼0.85; Gonzalez-Gutierrez and Grosman, 2010), and therefore, the possibility that a lower open probability in the absence of blocker underlies the much lower extent of block observed for ELIC can be completely ruled out.

Application of extracellular 5 mM lidocaine to ELIC, on the other hand, reduced the peak currents elicited by pulses of 10 mM cysteamine by a factor of ∼16 (mean peak current in the absence of lidocaine = 466 ± 109 pA, n = 16 patches; mean peak current in the presence of lidocaine = 29 ± 8 pA, n = 14 patches), and single-channel recordings also revealed a markedly reduced open probability (Fig. 6, A and B). Note, however, that a concentration

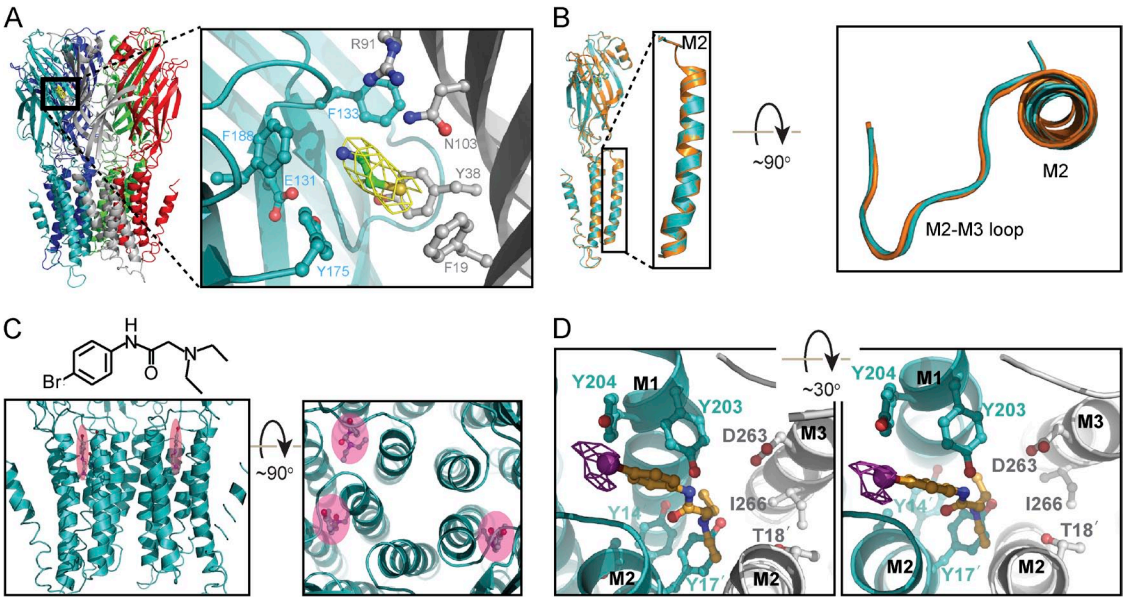

Figure 7. X-ray crystal structure of wild-type ELIC bound to cysteamine and either lidocaine or a brominated analogue. (A) Pentameric architecture of ELIC. The inset is a magnified view of the cysteamine-binding site with surrounding side chains shown in ball-and-stick representation. The carbon atoms of the amino acids forming the primary and secondary interfaces are represented in teal and gray, respectively. The yellow mesh represents the 2Fo–Fc electron-density map of cysteamine (carbon atoms, in green) contoured at the level of 1σ. The atoms of oxygen are shown in red; those of nitrogen, in blue; and those of sulfur, in yellow. (B) Structural alignment of wild-type ELIC cocrystalized with cysteamine and lidocaine (teal) with the previously solved model of unliganded wild-type ELIC (PDB code: 2VL0; orange); no change is apparent. For clarity, only one subunit is shown. The inset is a magnified view of the M2 α-helix and the M2–M3 loop. (C) Lateral and top views of the binding site for the bromo derivative N-1-(4-bromophenyl)-N-2,N-2 diethyl glycinamide (shadowed in pink). (D) A magnified view (from the extracellular side) of the bromo-derivative binding site; only two subunits are shown. Protein and brominated-analogue atoms are colored as in A, with the exception of the carbon atoms of the latter, which are shown in orange; the bromine atom is shown in purple. The anomalous-difference map corresponding to the bromo derivative (calculated at 4.8 Å and contoured at 4.5σ) is also displayed in purple. The amino acids in the M2 α-helices are denoted using the prime notation.

as high as 5 mM was needed for lidocaine to block ELIC to an extent that is similar to that achieved by 0.5 mM on the nAChR or GLIC (as judged from the reduction in the peak-current values). Regarding the decay of the macroscopic current in the presence of saturating agonist, application of extracellular lidocaine to ELIC had the opposite effect of that on the nAChR or GLIC: the time course was slowed down to the extent that no decline of the current was observed during 5-s pulses of 10 mM cysteamine in the continuous presence of 5 mM extracellular lidocaine (Fig. 6 A, inset, and Table 1). Puzzled by the strikingly different effects of lidocaine on the time courses of the current decay of the nAChR and GLIC, on the one hand, and that of ELIC, on the other, we set out to solve the crystal structure of ELIC in the presence of agonist (cysteamine) and either lidocaine or a brominated analogue. Although the structures were solved to a low resolution (≥3.65 Å; Table 2), the bromo derivative was clearly identified in the cavity lined by the back side of M2 and the front sides of M1 and M3 of several subunits (Fig. 7; the overall structure of ELIC, however, was not affected). Moreover, anomalous electron densities were found in these same regions (Fig. 7 D). Evidently, it would be important to determine whether and where lidocaine binds to the open-channel conformation of ELIC so as to be able to make a more direct comparison with the existing data on the binding of lidocaine (or its quaternary-ammonium derivatives) to the nAChR and GLIC (Leonard et al., 1988; Charnet et al., 1990; Hilf et al., 2010). It may well be that a given compound binds to different cavities of the channel in its different conformational states. Also, it is important to note that we have used lidocaine here only as a probe of structure–function relationships in a bacterial channel; our results should not be regarded as shedding light on the binding of anesthetics to their animal targets.

To probe the effect of structural perturbations to the lidocaine-binding site of ELIC, we engineered five single-point mutants (Y245A, Y248A, and T249A, in M2—corresponding to positions 14′, 17′, and 18′—and D263A and I266A, in M3; amino-acid numbering system as in Gonzalez-Gutierrez et al. [2012]) and one double mutant (Y203A + Y204A, in M1), and recorded their responses to 5-s pulses of a saturating concentration of agonist (Fig. 8). Three of these (Y203A + Y204A, T18′A, and D263A) failed to give rise to functional expression, I266A was wild-type-like (Table 3), and Y14′A and Y17′A displayed faster desensitization time courses (by factors of ∼17 and ∼12, respectively; Table 3) and lower open

TABLE 2

Data collection and refinement statistics

	ELIC + cysteamine + lidocaine	ELIC + cysteamine + brominated analog	ELIC + cysteamine + brominated analog
Data collection	P21	P21	P21
Space group			
Wavelength (Å)	0.97872	0.97872	0.91838
Cell dimensions			
a, b, c (Å)	104.96, 266.74, 110.60	105.58, 267.78, 110.43	105.89, 267.96, 110.29
α, β, γ (°)	90, 109.15, 90	90, 110.82, 90	90, 109.53, 90
Resolution (Å)	50–3.65 (3.78–3.65)	50–4.23 (4.38–4.23)	50–4.82 (4.99–4.82)
R_{sym}	0.123 (0.653)	0.112 (>1.0)	0.103 (0.716)
R_{meas}	0.134 (0.745)	0.122 (>1.0)	0.122 (0.856)
R_{pim}	0.051 (0.348)	0.069 (0.989)	0.065 (0.472)
$I/\sigma(I)$	13.6 (1.6)	8.6 (1.2)	10.4 (1.1)
Completeness (%)	98.9 (77.9)	97.9 (96.7)	96.3 (94.0)
Multiplicity	6.8 (3.5)	5.9 (4.9)	3.4 (2.9)
Refinement			
Resolution (Å)	49.58–3.65	48.75–4.23	
No. unique reflections	57,179	18,141	
R_{work}	0.235	0.256	
R_{free}	0.239	0.280	
Rmsd values			
Bond lengths (Å)	0.006	0.003	
Bond angles (°)	1.18	0.831	
No. atoms			
Protein	25,050	25,050	
Ligand	36	80	
Ramachandran plot			
Favored (%)	88.3	87.6	
Outliers (%)	3.5	3.3	

probabilities. The combination of these two single-point mutations into a double mutant gave rise to, essentially, the same phenotype (Fig. 8 and Table 3). We also tested the effect of 5 mM lidocaine on two of these mutants. When applied to the wild type-like I266A ELIC, lidocaine reduced the peak-current amplitude and slowed down the time course of current decay much like it did on the wild-type channel (Fig. 8 I). When applied to the loss-of-function Y14′A mutant, lidocaine decreased the peak-current amplitude to the extent that its effect on the current-decay time course could not be determined (Fig. 8 J). In summary, no mutation to the lidocaine-binding sites mimicked or prevented all the effects of lidocaine binding on channel function. However, the marked effects of the Y14′A and Y17′A mutations on the kinetics of desensitization and on the open probability in the presence of a saturating concentration of agonist does indicate that perturbations to the M1–M2–M3 cavity—caused by mutations, and perhaps, the binding of small molecules—can tilt the conformational free-energy landscape of ELIC.

Because pore block by extracellular quaternary-ammonium cations is one of the most characteristic properties of the cation-selective pLGICs, we were intrigued by our finding that 50 mM TEA^+ did not block the currents mediated by ELIC (Fig. 5, A and B). We reasoned that this lack of block could be the result of the open-channel pore of ELIC being too narrow to allow the access of a cation as large as TEA^+ (∼6.9 Å diam; Conway et al., 1966; Edward, 1970; Ue, 1994). Alternatively, at the other end of the spectrum of possibilities, the pore of ELIC in the open state could be wide enough and have the necessary electrostatic properties for TEA^+ to permeate nearly as fast as the mixture of K^+, Na^+, Ca^{2+}, and Mg^{2+} of our extracellular solution in such a way that the competition between TEA^+ and these inorganic cations would not result in a decreased conductance.

To test the possibility that the extracellular entrance to the transmembrane pore of ELIC is simply too narrow, we mutated the leucines at position 9′ and the phenylalanines at position 16′ to alanines and leucines, respectively, in an attempt to widen the pore cavity. The side chains at these two positions project into the lumen of the channel pore in the crystallized nonconductive conformation of ELIC (Hilf and Dutzler, 2008) and are likely to also do so in the open-channel conformation; in the muscle nAChR, they certainly do (Cymes et al., 2005). As was the case for wild-type ELIC, however, neither the peak value of the macroscopic currents nor the time course of the current response recorded from the

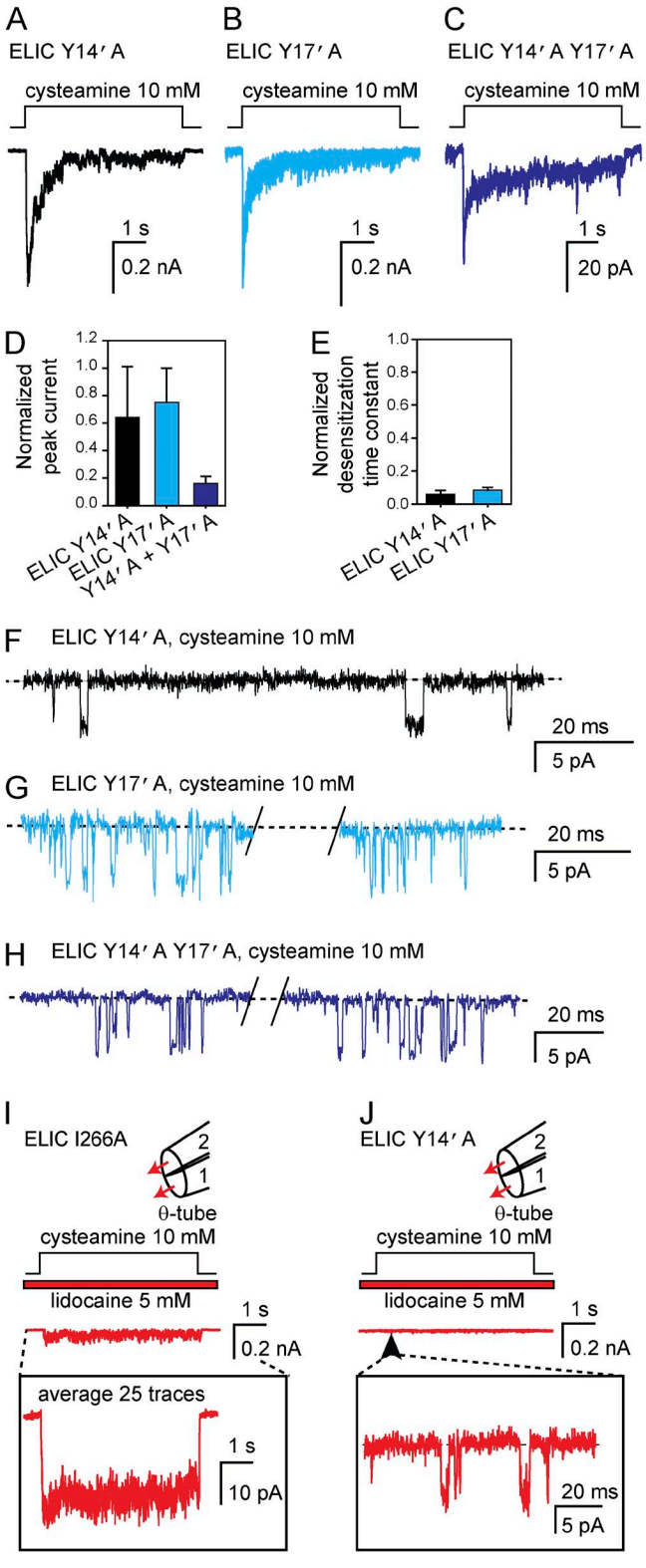

Figure 8. Effects of mutations to the lidocaine-binding site of ELIC. (A–C) Macroscopic current responses to 5-s pulses of 10 mM cysteamine recorded at –80 mV from 3 M2 α-helix mutants in the outside-out configuration. The solutions flowing through the two barrels of the perfusion tubing were (in mM) 142 KCl, 5.4 NaCl, 1.8 $CaCl_2$, 1.7 $MgCl_2$, and 10 HEPES/KOH, pH 7.4, with or without cysteamine. The trace shown in C is the average of 27 responses recorded from 7 patches. (D and E) Peak-current amplitudes and time constants of desensitization normalized to wild-type values. The plotted values are means obtained from 3 (Y14′A), 4 (Y17′A), and 7 (Y14′A + Y17′A) patches; error bars are the corresponding standard errors. The desensitization time courses recorded from the Y14′A + Y17′A double mutant had low peak-current amplitudes, and hence, a total of 27 traces from 7 patches were averaged and fitted (Table 3); a proper fit required two (rather than one) exponential-decay components. (F–H) Single-channel inward currents elicited by 10 mM cysteamine recorded at –80 mV in the outside-out configuration; openings are downward deflections. The external solution was (in mM) 142 KCl, 5.4 NaCl, 1.8 $CaCl_2$, 1.7 $MgCl_2$, 10 cysteamine, and 10 HEPES/KOH, pH 7.4. For comparison, single-channel traces recorded from the wild-type channel under identical experimental conditions are shown in Fig. 6 B, top. (I and J) Macroscopic current responses to 5-s pulses of 10 mM cysteamine in the continuous presence of 5 mM lidocaine recorded at –80 mV from 2 mutants (in the M3 and M2 α-helices, respectively) in the outside-out configuration. The solutions flowing through the two barrels of the perfusion tubing were as in A–C, with the addition of 5 mM lidocaine. In the schematic representation of the theta-tubing perfusion, arrows indicate the application of lidocaine.

L9′A + F16′L double mutant was affected by the continuous presence of extracellular TEA^+ at a concentration as high as 50 mM (Fig. 9, A and B; and Table 1). The same was the case for TMA^+ (a smaller cation, ∼5.7 Å diam; Conway et al., 1966; Edward, 1970; Ue, 1994) on both the wild-type and the L9′A + F16′L wider-pore mutant at a concentration of 50 mM (Fig. 9, C–E; and Table 1). To emphasize the atypical properties of ELIC, Fig. 10 illustrates the blocking effect of TMA^+ on the nAChR at the macroscopic and single-channel levels when also applied to the extracellular side at a concentration of 50 mM. TMA^+ is both a fast pore blocker and an agonist of the nAChR.

Regarding the open probability between desensitized intervals of the L9′A + F16′L mutant of ELIC in the presence of 10 mM cysteamine and the absence of quaternary-ammonium cations, we note that its value (∼0.45; Gonzalez-Gutierrez et al., 2012) is lower than the muscle-nAChR's (∼0.85 in the presence of 100-µM ACh and the absence of quaternary-ammonium cations; Gonzalez-Gutierrez and Grosman, 2010) only by a factor of ∼1.9. In other words, although lower, this open probability is not low enough to account for the negligible block of this double mutant by 50 mM TEA^+ or TMA^+.

Quaternary-ammonium cations carry measurable currents through ELIC

To test the possibility that TMA^+ can conduct measurable currents through ELIC, we replaced the extracellular mixture of K^+, Na^+, Ca^{2+}, and Mg^{2+} present in the agonist-containing barrel of the theta-type tubing of our perfusion system with a solution containing TMA^+ and agonist alone. More specifically, this solution consisted of (in mM) 142 TMACl, 10 cysteamine chloride, and

TABLE 3

Effect of mutations to the lidocaine binding site of ELIC on the time course of desensitization

Channel	$\tau_{desensitization}$		P-value	Number of patches
	(mean ± SE; ms)	(range; ms)		
Wild-type ELIC	4,533 ± 584	2,397–8,026	–	9
I266A ELIC	6,324 ± 1,132	2,834–8,081	0.11	5
Y14′A ELIC	272 ± 96	146–415	1.5×10^{-3}	3
Y17′A ELIC	383 ± 64	282–541	4.7×10^{-4}	4
Y14′A + Y17′A ELIC[a]	112 (56%)	–	–	7
	4,820	–		

[a]The macroscopic recordings obtained from this double mutant had low peak-current amplitudes. Hence, we averaged 27 responses from 7 different outside-out patches to obtain a proper fit; the desensitization time course was fitted adequately with two exponential components. In an attempt to compare these double-exponential kinetics with the mono-exponential kinetics of the wild type and single mutants, we calculated the corresponding decay half-times. These values were as follows (in ms): 3,142, 189, 265, and 219 for wild-type, Y14′A, Y17′A, and Y14′A + Y17′A ELIC, respectively.

10 HEPES/TMAOH, pH 7.4; the solution flowing through the other barrel of the theta tube (that is, the agonist-free solution) remained unchanged (in mM: 142 KCl, 5.4 NaCl, 1.8 $CaCl_2$, 1.7 $MgCl_2$, and 10 HEPES/KOH, pH 7.4). To allow for a comparison across channel types, we also applied this type of pulse protocols to the nAChR and GLIC. Because TMA^+ is a high-efficacy agonist of the nAChR, no additional ligands were added to the TMA^+-containing solution when assaying this channel. In the case of GLIC, the pH of the 142-mM TMA^+ solution was buffered with 10 mM acetic acid (instead of HEPES), and its value was adjusted to 4.5 with TMAOH.

The responses of the nAChR and GLIC are illustrated in Fig. 11, whereas that of ELIC is illustrated in Fig. 12. In the case of the nAChR, the ratio between the macroscopic current values before and after TMA^+ removal was ∼0.08, thus suggesting that TMA^+ carries a current that is ∼8.0% of that carried by the mixture of K^+, Na^+, Ca^{2+}, and Mg^{2+} present in the agonist-free solution (Fig. 11 A). Because the fast deactivation of the nAChR (time constant = 1.1 ± 0.1 ms; $n = 12$) could have led to an underestimation of the peak-value reached upon TMA^+ removal, we repeated this type of experiment with a mutant nAChR that deactivates more slowly (εT12′P; Ohno et al., 1995); in this case, the ratio was estimated to be ∼0.01 (Fig. 11 B). In other words, a value of ∼1% seems to be a more accurate estimate of the ratio of the current carried by TMA^+ through the nAChR relative to the current carried by the mixture of K^+, Na^+, Ca^{2+}, and Mg^{2+}. In the case of GLIC, the response was very similar to that of the nAChR: we found the corresponding ratio to be ∼0.02 (Fig. 11 C), although, owing to the fast deactivation time course of GLIC (time constant = 0.91 ± 0.20 ms, in the absence of TMA^+; $n = 11$), this number is likely to be an upper bound. Fig. 11 D summarizes the numerical values obtained from these experiments.

In striking contrast, the ratio of intra–pulse-to-tail current values corresponding to ELIC was much larger than those obtained for the nAChR or GLIC. Indeed, this ratio was ∼0.25 for wild-type ELIC and ∼0.35 for the wider-pore mutant (Fig. 12, A–C). We also measured the amplitude of inward single-channel currents elicited by 10 mM cysteamine at –80 mV in outside-out patches bathed by either the K^+-Na^+-Ca^{2+}-Mg^{2+} solution or the 142-mM TMA^+ solution on the extracellular side (Fig. 12 D). Under these conditions, we found the ratio of unitary-current amplitudes of wild-type ELIC to be 0.22 ± 0.01 ($n = 13$), a value that is very similar to that estimated from macroscopic current recordings (Fig. 12, A–C). Similar attempts to record single-channel currents carried by TMA^+ alone through the nAChR or GLIC proved unsuccessful, which is hardly surprising given the small amplitude of the macroscopic currents shown in Fig. 11.

We also tested whether TEA^+ permeates through the pore of ELIC. Using the same type of pulse protocol as that illustrated for TMA^+ in Fig. 12 (A and B), we found the ratio between the current value reached at the end of the pulse of TEA^+ plus agonist and the peak value reached upon switching the external solution to the mixture of K^+, Na^+, Ca^{2+}, and Mg^{2+} to be ∼0.09 (Fig. 12 E). That is, with a solution containing (in mM) 142 TEACl, 10 cysteamine chloride, and 10 HEPES/TEAOH, pH 7.4 on the extracellular side, the inward currents were as large as ∼9% of their value when the extracellular solution consisted of (in mM) 142 KCl, 5.4 NaCl, 1.8 $CaCl_2$, 1.7 $MgCl_2$, and 10 HEPES/KOH, pH 7.4. Nearly the same value (∼0.10) was obtained with the L9′A + F16′L double mutant of ELIC (Fig. 12, F and G), indicating that the larger side chains of leucine at position 9′ and phenylalanine at position 16′ do not affect the rate of TEA^+ permeation through the channel. Collectively, the results with TMA^+ and TEA^+ strongly suggest that, in the open-channel conformation, the pore of ELIC is wider at its narrowest constriction than are the pores of the muscle nAChR or GLIC.

Although TMA^+ and TEA^+ permeate faster through ELIC than they do through the nAChR or GLIC, as previously mentioned, the currents these cations carry through ELIC when present as the only extracellular

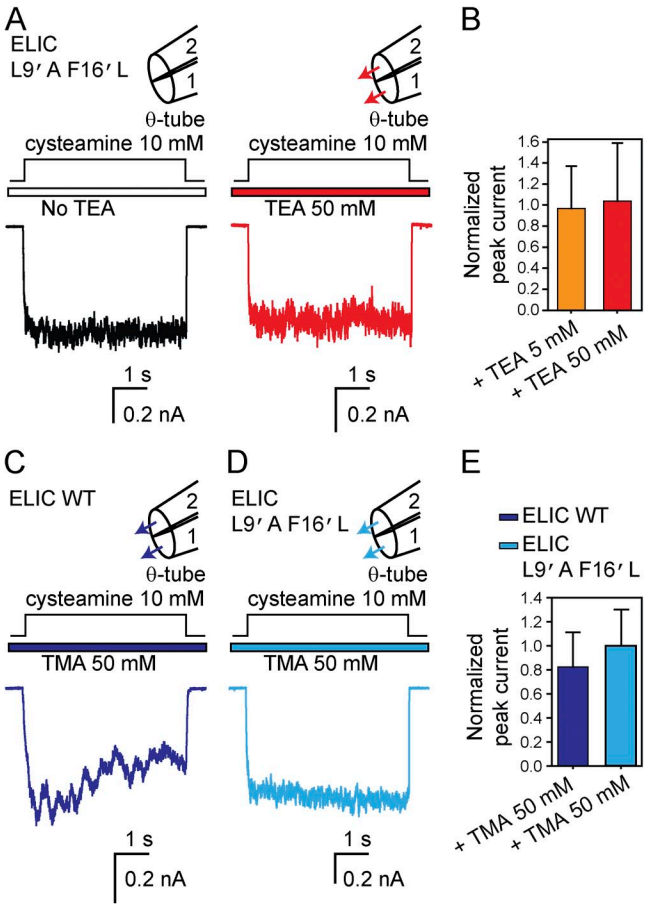

Figure 9. 50 mM TEA^+ or TMA^+ fail to block wild-type ELIC and a wider-pore mutant. (A) Macroscopic current responses to 5-s pulses of 10 mM cysteamine recorded from the L9′A + F16′L wider-pore mutant at –80 mV in the outside-out configuration. The responses were recorded without TEA^+ in either barrel or in the presence of 50 mM TEA^+ flowing through both barrels of the theta-type perfusion tubing. Because ELIC displayed marked rundown in outside-out patches, these traces were not recorded sequentially. Instead, individual patches of membrane were exposed to cysteamine pulses either in the absence or the presence of TEA^+. The solutions flowing through the two barrels of the perfusion tubing were (in mM) 142 KCl, 5.4 NaCl, 1.8 $CaCl_2$, 1.7 $MgCl_2$, and 10 HEPES/KOH, pH 7.4, with or without cysteamine and with or without TEA^+. In the schematic representations of the theta-tubing perfusion, arrows indicate the application of TEA^+. (B) Peak-current amplitudes recorded in response to the application of cysteamine in the presence of external 5 or 50 mM TEA^+ normalized to the peak value observed in the absence of TEA^+. The plotted values are means obtained from 4 (5 mM TEA^+) and 7 (50 mM TEA^+) patches; error bars are the corresponding standard errors. (C and D) Macroscopic current responses to 5-s pulses of 10 mM cysteamine in the presence of external 50 mM TMA^+ recorded from the wild type and the L9′A + F16′L mutant at –80 mV in the outside-out configuration. All other conditions are as in A, replacing TEA^+ with TMA^+. The corresponding responses in the absence of TMA^+ are shown in Fig. 5 A (for the wild type) and in panel A of this figure (for the mutant). (E) Peak-current amplitudes recorded in response to the application of cysteamine in the presence of external 50 mM TMA^+ normalized to the peak value observed in the absence of TMA^+. The plotted values are means obtained from 9 (wild-type ELIC) and 8 (L9′A + F16′L mutant) patches; error bars are the corresponding standard errors.

cations are nevertheless smaller than the current carried by the mixture of K^+, Na^+, Ca^{2+}, and Mg^{2+} (by a factor of ∼3–4 in the case of TMA^+ and ∼11 in the case of TEA^+). However, the addition of TMA^+ or TEA^+ (up to a concentration of 50 mM) to the K^+-Na^+-Ca^{2+}-Mg^{2+} solution had hardly any effect on the size of the peak-current amplitudes carried by this mixture of inorganic cations alone (Figs. 5 and 9). Thus, this lack of blockade by TMA^+ or TEA^+ cannot be ascribed to the channel being too narrow to enter the pore (because these cations certainly conduct currents) or to TMA^+ and TEA^+ permeating as fast as the mixture of inorganic cations (because the currents carried by TMA^+ and TEA^+ are smaller). Thus, it seems as though the only explanation for the lack of current block illustrated in Figs. 5 and 9 is that TMA^+ and TEA^+ interact with the open-channel pore of ELIC with such low affinity that the other cations also present in the extracellular solution—that is, K^+ (142 mM), Na^+ (5.4 mM), Ca^{2+} (1.8 mM), and Mg^{2+} (1.7 mM)—outcompete them, at least when TMA^+ and TEA^+ are present at a concentration of 50 mM. To test this idea, we repeated the competition experiments now using a higher concentration of TEA^+ and a simpler background solution (Fig. 13). More specifically, the TEA^+-containing solution consisted of (in mM): 142 KCl, 142 TEACl, 10 cysteamine chloride, and 10 HEPES/KOH, pH 7.4; the solution flowing through the other barrel of the theta tube (that is, the TEA^+-free solution) consisted of (in mM): 142 KCl and 10 HEPES/KOH, pH 7.4. Under these conditions, we found that the current carried by the equimolar TEA^+-K^+ solution was ∼53% of that recorded upon TEA^+ removal, i.e., in the presence of 142 mM K^+ alone, in the case of the wild type, and ∼54% in the case of the wider-pore mutant (Fig. 13 C). Evidently, a higher concentration of TEA^+ is required to block K^+ currents through ELIC than is required in the case of the nAChR or GLIC. Finally, we reasoned that—when present at the same concentration—a quaternary-ammonium cation larger than TEA^+ would block K^+ currents to a larger extent. As shown in Fig. 14, this expectation was fully borne out by experiments with 142 mM tetrapropylammonium (TPA^+) chloride (TPACl; Fig. 14 A); in the presence of an equimolar mixture of KCl and TPACl (both at a concentration of 142 mM) applied to the extracellular side of ELIC, the current was ∼30% as large as that carried by the K^+ solution alone. Fig. 14 also shows that 142 mM TPA^+ carries a small but measurable current through ELIC when present as the only cation on the extracellular side (amounting to ∼3.5% of the current carried by the mixture of K^+, Na^+, Ca^{2+}, and Mg^{2+} alone; Fig. 14 B), which is intriguing in light of the large diameter of this cation (∼7.8 Å; Conway et al., 1966; Edward, 1970; Ue, 1994).

It may be argued that the cation-conduction properties of ELIC could have been characterized much more directly and in more quantitative detail at the single-channel

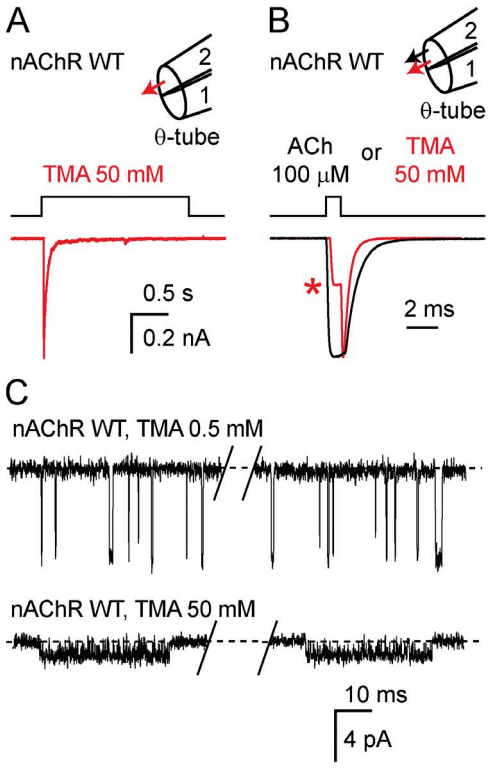

Figure 10. Block of the muscle nAChR by TMA^+. (A) Macroscopic current response to a 2-s pulse of 50 mM TMA^+ recorded at –80 mV from the mouse muscle adult-type nAChR in the outside-out configuration. Because TMA^+ is both a pore blocker and a (desensitizing) agonist of the nAChR, TMA^+ was applied only transiently rather than continuously (compare with Fig. 9, C and D). The solutions flowing through the two barrels of the perfusion tubing were (in mM) 142 KCl, 5.4 NaCl, 1.8 $CaCl_2$, 1.7 $MgCl_2$, and 10 HEPES/KOH, pH 7.4, with or without TMA^+. In the schematic representation of the theta-tubing perfusion, the arrow indicates the application of TMA^+. (B) Macroscopic current responses to a 1-ms pulse of 100-μM ACh or 50 mM TMA^+ recorded at –80 mV in the outside-out configuration. The solutions flowing through the two barrels of the perfusion tubing were as described in A with or without ACh and with or without TMA^+. The two traces are averages of 10 consecutive responses recorded from two separate representative patches and were normalized for displaying purposes in such a way that the current values attained upon ligand removal are the same; this emphasizes the block by TMA^+ (see red asterisk). In the schematic representation of the theta-tubing perfusion, arrows indicate the application of ACh or TMA^+. (C) Single-channel inward currents elicited by 0.5 mM or 50 mM TMA^+ recorded at approximately –100 mV in the cell-attached configuration; openings are downward deflections. The pipette solution was (in mM) 142 KCl, 5.4 NaCl, 1.8 $CaCl_2$, 1.7 $MgCl_2$, 0.5 or 50 TMA^+, and 10 HEPES/KOH, pH 7.4. The extent of block caused by TMA^+ seems to be larger in the single-channel recordings than in the macroscopic recordings. Undoubtedly, this is due to the fast deactivation time constant of the nAChR, which leads to the underestimation of the true peak value of the macroscopic transient upon TMA^+ removal.

level. However, here, we specifically wanted to contrast these properties with those of the nAChR and GLIC, and given the low unitary conductance of the latter (even in the absence of blockers), this would have been nearly impossible to achieve using single-channel recordings. Thus, we felt that it was desirable to consider an experimental design that could be applied to all three channels under the same experimental conditions. The importance of including a second bacterial channel in the comparison seemed to fully justify the more indirect nature of macroscopic recordings.

Leucine-to-alanine mutations at position 9′ speed up the deactivation of ELIC

To gain insight into the interconversion among the closed, open, and desensitized states of ELIC, we compared the effects of reducing the hydrophobicity of the pore lining on the kinetics of deactivation. Channel deactivation is the decay of the macroscopic current that occurs on agonist removal, and thus, its kinetics depend on the rates of agonist dissociation and closed–open–desensitized state interconversions, with the contribution of each of these rates varying among different channels (Jones and Westbrook, 1995; Elenes et al., 2006). On the other hand, for channels that activate much faster than they desensitize, the kinetics of desensitization measured at saturating concentrations of agonist—that is, the kinetics of the macroscopic current decay that occurs during the application of agonist—depend on the rates at which the channel enters and leaves the desensitized state(s) while fully bound to the ligand. Thus, the time courses of deactivation and desensitization reflect different (although somewhat overlapping) sets of rates.

For these experiments, we chose the side chain at position 9′ (a leucine in all subunits of the muscle nAChR and ELIC, and an isoleucine in GLIC) because the effect of mutations at this position on the kinetics of deactivation—or, its single-molecule equivalent, the mean duration of bursts of single-channel openings (Wyllie et al., 1998)—has been extensively documented for the pLGICs from vertebrates (for example: Filatov and White, 1995; Labarca et al., 1995; Chang and Weiss, 1998; Kosolapov et al., 2000; Bianchi and Macdonald, 2001; Papke and Grosman, 2014). Fig. 15 illustrates the effect of shortening these side chains by mutation to alanine in the muscle nAChR and GLIC. The presence of a mutant alanine at this position of the two α subunits of the nAChR and in all five subunits of GLIC slowed down deactivation (by factors of ∼90 and ∼178, respectively; Table 4), a phenomenon shared by all other pLGICs for which the effect of this type of mutation on deactivation has been recorded. However, in ELIC, the leucine-to-alanine mutation sped up deactivation, with the time constant of the monoexponential fit being shortened by a factor of ∼3.5 (Fig. 16 and Table 4; see also Gonzalez-Gutierrez et al., 2012). To rule out the possibility that the phenylalanine at the pore-lining position 16′ of ELIC has anything to do with this unexpected behavior (indeed, five phenylalanines at this

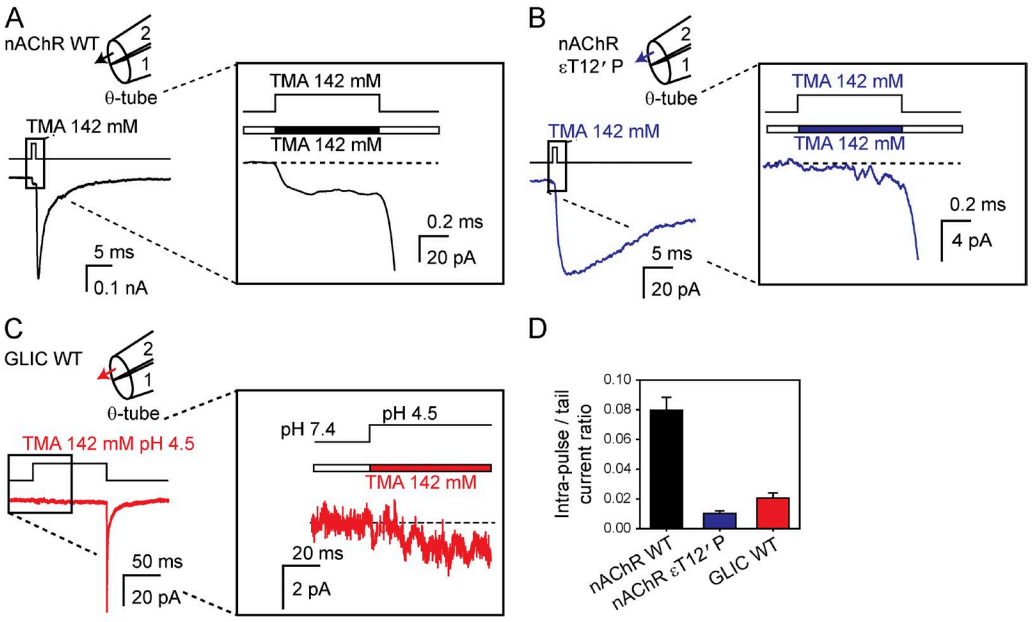

Figure 11. TMA^+ conduction through the muscle nAChR and GLIC. (A and B) Macroscopic current responses to 1-ms pulses of 142 mM TMA^+ recorded at –80 mV from the wild-type (A) and the εT12′P slowly deactivating mutant (B) of the mouse muscle adult-type nAChR in the outside-out configuration. The TMA^+-containing solution was (in mM) 142 TMACl and 10 HEPES/TMAOH, pH 7.4, whereas the TMA^+-free solution was (in mM) 142 KCl, 5.4 NaCl, 1.8 $CaCl_2$, 1.7 $MgCl_2$, and 10 HEPES/KOH, pH 7.4. In the schematic representations of the theta-tubing perfusion, arrows indicate the application of TMA^+. (C) Macroscopic current response to a 100-ms pulse of pH-4.5 solution ($pH_{holding}$ 7.4) containing 142 mM TMA^+ recorded at –80 mV from GLIC in the outside-out configuration. The TMA^+-containing solution was (in mM) 142 TMACl and 10 acetic acid/TMAOH, pH 4.5, whereas the TMA^+-free solution was (in mM) 142 KCl, 5.4 NaCl, 1.8 $CaCl_2$, 1.7 $MgCl_2$, and 10 HEPES/KOH, pH 7.4. The short duration of the pH-4.5-solution application ensured that entry into desensitization within the pulse was negligible. All other conditions are as in A and B. (D) Intra–pulse-to-tail current ratios. The plotted values are means obtained from 17 (wild-type nAChR), 11 (εT12′P nAChR), and 6 (GLIC) patches; error bars are the corresponding standard errors. All current traces shown in this figure are the averages of 10 consecutive responses recorded from representative patches.

position seem to occur only in some bacterial and invertebrate homologues whose functional properties have not been extensively characterized yet), we also recorded the deactivation time course of the wider-pore L9′A + F16′L mutant that we used in our previously mentioned permeation studies; a leucine at position 16′ is present in four of the five subunits of the muscle nAChR, whereas an isoleucine at this position is present in all five subunits of GLIC. Remarkably, the deactivation time course of this double mutant of ELIC was faster too, also by a factor of ∼3.5 (Fig. 16, C and F; and Table 4; Gonzalez-Gutierrez et al., 2012). Mutating the leucine at position 9′ of ELIC to glutamine or glutamate—two polar amino acids—in the wild-type background gave rise to, essentially, the same result: these mutations did not slow down the deactivation time course of ELIC (Fig. 16, D–F; and Table 4).

As for desensitization, the effect of mutating the leucine at position 9′ of ELIC to alanine (both in the wild-type and the F16′L backgrounds) was unremarkable: the decay of the macroscopic current became much slower, to the extent of being negligible during the 5-s applications of 10 mM cysteamine (Fig. 9 A), largely as observed for the muscle nAChR (Filatov and White, 1995; Papke and Grosman, 2014), GLIC (Bocquet et al., 2007; Gonzalez-Gutierrez et al., 2012), and all other pLGICs examined to date (e.g., Bianchi and Macdonald, 2001).

Collectively, the effects of mutations at position 9′ of the nAChR and GLIC on the time courses of deactivation and desensitization suggest that reducing the hydrophobicity of the transmembrane pore-lining destabilizes the closed and desensitized states of these two channels relative to the open state. (Although changes in the agonist-dissociation rate constant would have contributed to affect the kinetics of deactivation, we deem it unlikely for a mutation in the middle of the M2 α-helix to affect the unbinding kinetics from the distant transmitter-binding sites.) This proposed relative stabilization of the open state is consistent with the longer clusters of single-channel openings and the higher closed-to-open gating equilibrium constant of nAChR 9′ mutants inferred from unitary currents recorded at saturating concentrations of agonist (Cymes et al., 2002). In marked contrast, the same experimental maneuvers applied to ELIC destabilize the open and the desensitized states, with the destabilization of the latter being larger. That the open state of ELIC becomes

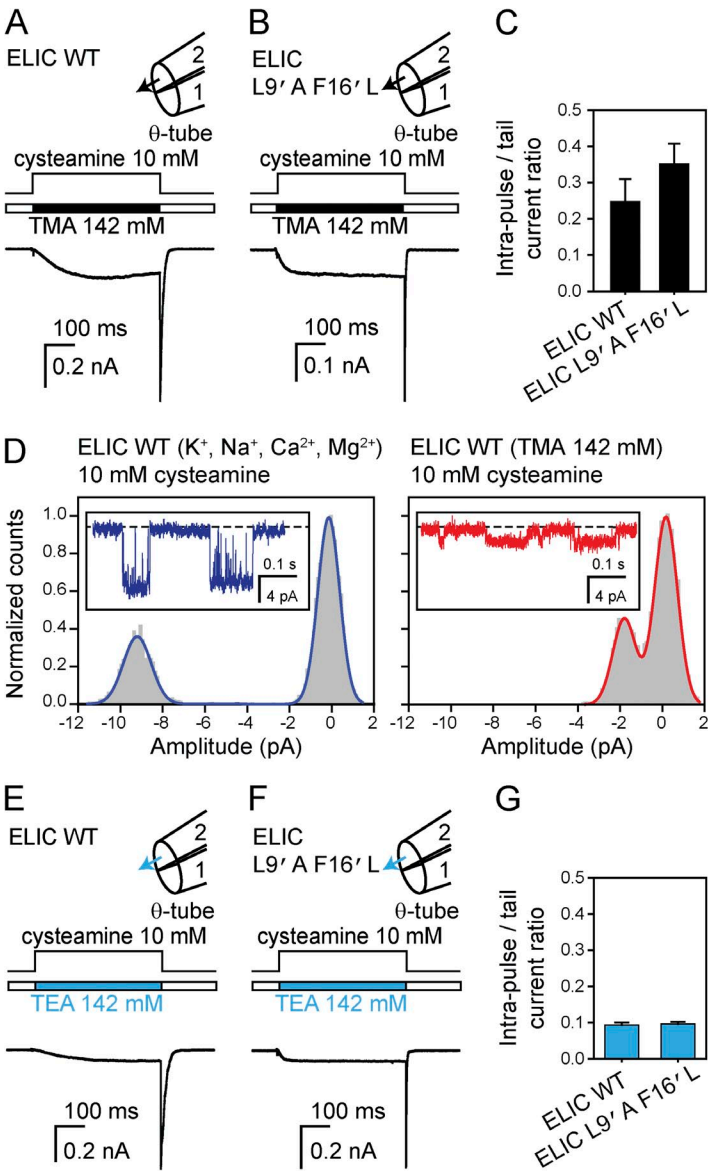

Figure 12. TMA^+ and TEA^+ conduction through ELIC. (A and B) Macroscopic current responses to 500-ms pulses of 10 mM cysteamine plus 142 mM TMA^+ recorded at –80 mV from the wild type (A) and the L9′A + F16′L wider-pore mutant (B) in the outside-out configuration. The TMA^+-containing solution was (in mM) 142 TMACl, 10 cysteamine, and 10 HEPES/TMAOH, pH 7.4, whereas the TMA^+-free solution was (in mM) 142 KCl, 5.4 NaCl, 1.8 $CaCl_2$, 1.7 $MgCl_2$, and 10 HEPES/KOH, pH 7.4. In the schematic representations of the theta-tubing perfusion, arrows indicate the application of TMA^+. (C) Intra–pulse-to-tail current ratios. The plotted values are means obtained from 5 (wild type) and 6 (L9′A + F16′L mutant) patches; error bars are the corresponding standard errors. (D) Single-channel inward currents elicited by 10 mM cysteamine recorded at –80 mV in the outside-out configuration (openings are downward deflections) and corresponding all-point amplitude histograms. For the panel on the left, the external solution was (in mM) 142 KCl, 5.4 NaCl, 1.8 $CaCl_2$, 1.7 $MgCl_2$, 10 cysteamine, and 10 HEPES/KOH, pH 7.4, whereas for the panel on the right, this solution was (in mM) 142 TMACl, 10 cysteamine, and 10 HEPES/TMAOH, pH 7.4. (E–G) Macroscopic current responses and intra–pulse-to-tail current ratios. All conditions are as in (A–C), replacing TMA^+ with TEA^+. The values plotted in G are means obtained from 9 (wild type) and 7 (L9′A + F16′L mutant) patches; error bars are the corresponding standard errors. All macroscopic current traces shown in this figure are the averages of 10 consecutive responses recorded from representative patches.

destabilized relative to the closed state upon mutation was also evident at the single-channel level, in recordings performed at saturating concentrations of cysteamine that showed an intracluster open probability lower than the wild-type's (Gonzalez-Gutierrez et al., 2012).

Admittedly, we have not tested the effect of all other natural side chains at position 9′ of ELIC, but the results obtained with alanine, glutamine, and glutamate seem compelling enough to conclude that, in this channel, the relationship between pore hydrophobicity, pore-water content, and the relative stabilities of the closed, open, and desensitized states is quite unique. To our knowledge, ELIC is the only pLGIC studied to date that deviates from the rule that mutations that reduce the hydrophobicity of the transmembrane pore lining stabilize the open-channel conformation relative to both the closed and desensitized states.

A more polar lining increases the affinity of ELIC's pore for cysteamine

The responses of the glutamine and glutamate mutants of ELIC to cysteamine pulses (Fig. 16, D and E) differed from those recorded from the other tested constructs (Fig. 16, A–C) in that the currents transiently rose upon cysteamine removal. The solutions alternately bathing the outside-out patches in these experiments were the K^+-Na^+-Ca^{2+}-Mg^{2+} solution with or without 10 mM cysteamine, and thus, the observed current overshoots indicate that this agonist blocked the currents carried by these two mutants to some extent (with pK_{a1} and pK_{a2} values of ∼8.3 and ∼10.8 [Avdeef and Brown, 1984], a 10-mM cysteamine solution at pH 7.4 is expected to contain ∼8.9 mM of the doubly protonated, positively charged form). However, a careful examination of the electrophysiological responses recorded from the wild

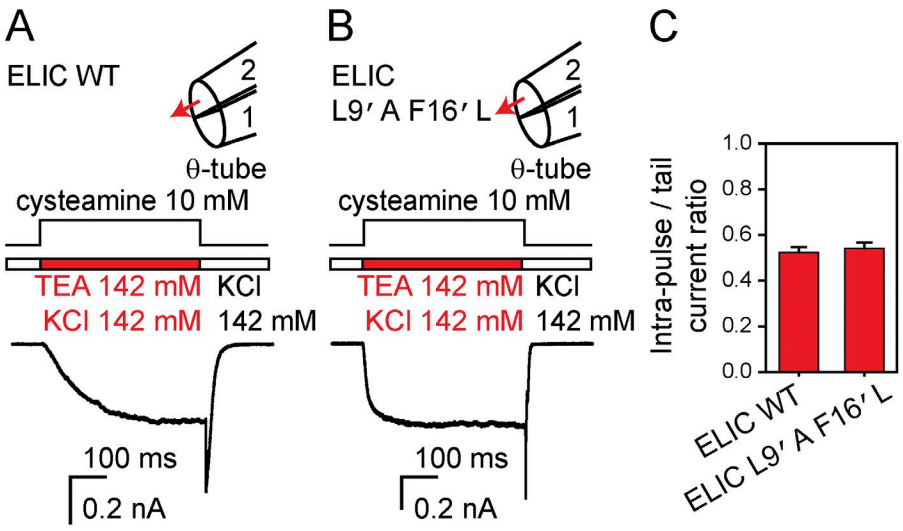

Figure 13. TEA^+–K^+ competition in ELIC. (A and B) Macroscopic current responses to 500-ms pulses of 10 mM cysteamine plus 142 mM TEA^+ recorded at –80 mV from the wild type (A) and the L9′A + F16′L wider-pore mutant (B) in the outside-out configuration. The TEA^+-containing solution was (in mM) 142 KCl, 142 TEACl, 10 cysteamine, and 10 HEPES/KOH, pH 7.4, whereas the TEA^+-free solution was (in mM) 142 KCl and 10 HEPES/KOH, pH 7.4. In the schematic representations of the theta-tubing perfusion, arrows indicate the application of TEA^+. (C) Intra–pulse-to-tail current ratios. The plotted values are means obtained from 9 (wild type) and 3 (L9′A + F16′L mutant) patches; error bars are the corresponding standard errors. Both current traces shown in this figure are the averages of 10 consecutive responses recorded from two representative patches.

type, the L9′A single mutant, and the L9′A + F16′L double mutant failed to reveal such fast block by cysteamine, which is important in the context of this paper because these were the variants of ELIC that we used for the permeation studies described above. Therefore, our decision to disregard the presence of 10 mM cysteamine in the experiments that probed the permeation properties of ELIC is fully justified. Clearly, it seems as though the presence of a more polar lining in the L9′Q and L9′E mutants of ELIC increases the affinity of the pore for the, also polar, cysteamine.

DISCUSSION

Before this work, the characterization of two bacterial pLGICs had suggested that the functional properties of the noneukaryotic members of the superfamily fell well within the range of variability revealed by decades of

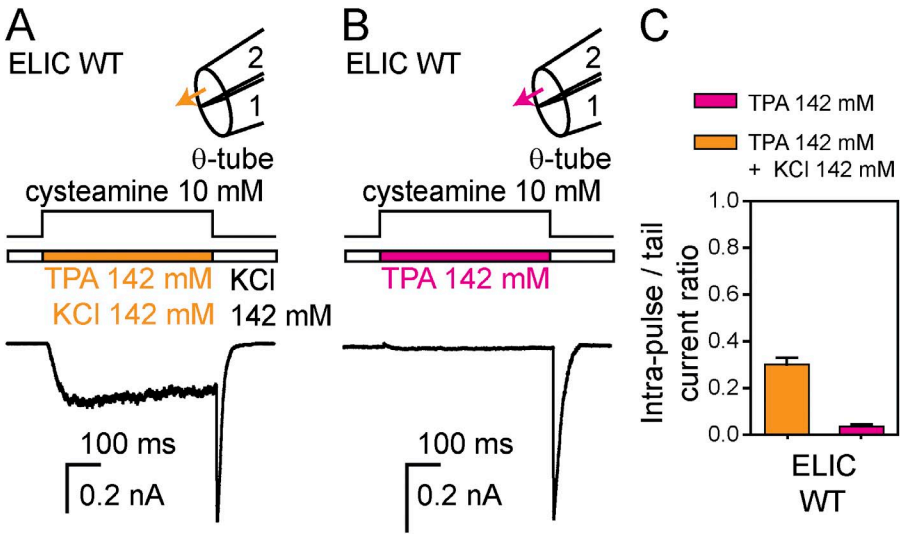

Figure 14. TPA^+–K^+ competition and TPA^+ conduction through ELIC. (A and B) Macroscopic current responses to 500-ms pulses of 10 mM cysteamine plus 142 mM TPA^+ recorded at –80 mV from the wild type in the outside-out configuration. In (A), the TPA^+-containing solution was (in mM) 142 KCl, 142 TPACl, 10 cysteamine, and 10 HEPES/KOH, pH 7.4, whereas the TPA^+-free solution was (in mM) 142 KCl and 10 HEPES/KOH, pH 7.4. In (B), the TPA^+-containing solution was (in mM) 142 TPACl, 10 cysteamine, and 10 HEPES/TPAOH, pH 7.4, whereas the TPA^+-free solution was (in mM) 142 KCl, 5.4 NaCl, 1.8 $CaCl_2$, 1.7 $MgCl_2$, and 10 HEPES/KOH, pH 7.4. In the schematic representations of the theta-tubing perfusion, arrows indicate the application of TPA^+. (C) Intra–pulse-to-tail current ratios. The plotted values are means obtained from 5 patches for each condition; error bars are the corresponding standard errors. Both current traces shown in this figure are the averages of 10 consecutive responses recorded from two representative patches.

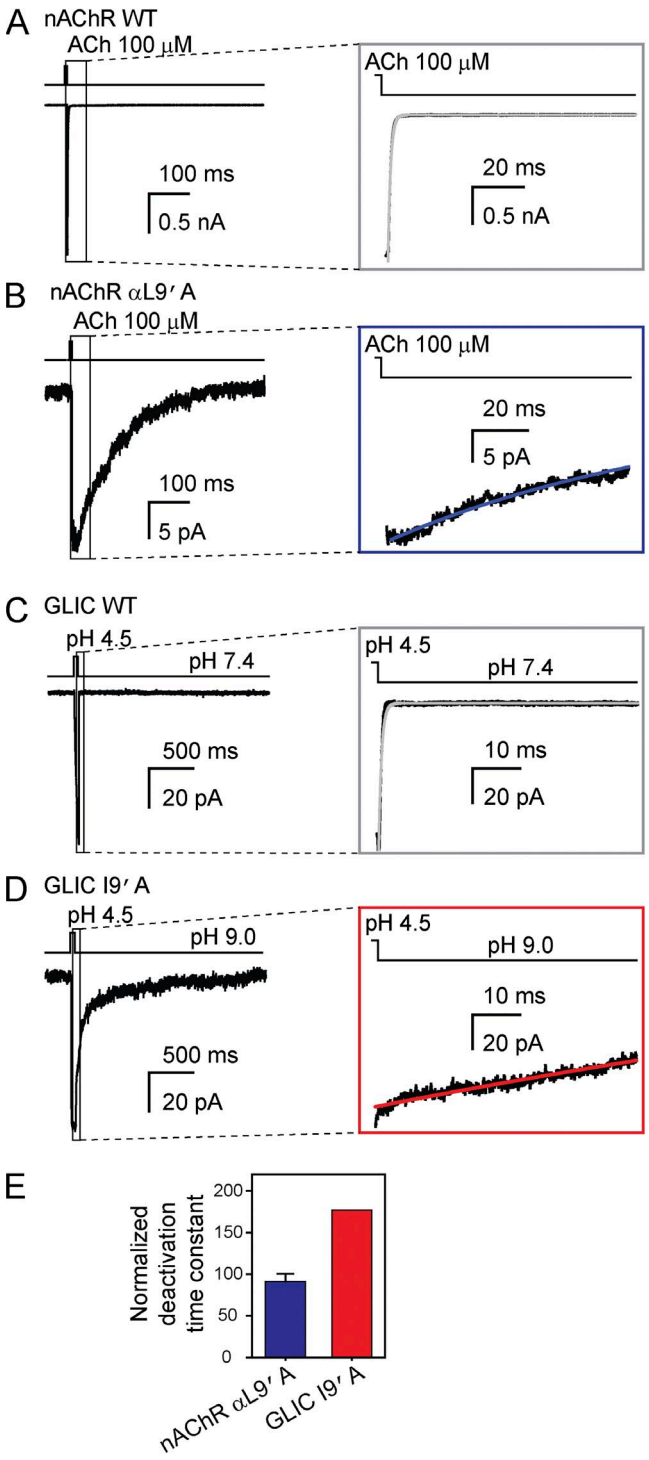

Figure 15. Effect of mutations at position 9′ of M2 on deactivation of the muscle nAChR and GLIC. (A and B) Macroscopic current responses to 1-ms pulses of 100-μM ACh recorded at –80 mV from the wild-type mouse muscle adult-type nAChR (A) and the αL9′A mutant (B) in the outside-out configuration. The solutions flowing through the two barrels of the perfusion tubing were (in mM) 142 KCl, 5.4 NaCl, 1.8 $CaCl_2$, 1.7 $MgCl_2$, and 10 HEPES/KOH, pH 7.4, with or without ACh. (C and D) Macroscopic current responses to 50-ms pulses of pH-4.5 solution recorded at –80 mV from wild-type GLIC (C) and the I9′A mutant (D) in the outside-out configuration. The solutions flowing through the two barrels of the perfusion tubing were (in mM) 142 KCl, 5.4 NaCl, 1.8 $CaCl_2$, 1.7 $MgCl_2$, and the pH was buffered with 10 HEPES/KOH (pH 7.4), 10 TABS/KOH (pH 9.0) or 10 acetic-acid/KOH (pH 4.5). In the case of the gain-of-function I9′A mutant, the (proton-gated) activity of the channel at pH 7.4 was relatively high, and hence, the pH of the solution applied during the "no-agonist" intervals was increased to 9.0. For all panels, the insets emphasize the time courses of deactivation; lines are fits to monoexponential-decay functions. (E) Mutant-construct deactivation time constants obtained from monoexponential fits normalized to the corresponding wild-type time constants. The plotted values are means obtained from 4 (L9′A nAChR) and 2 (I9′A GLIC) patches. An error bar (standard error) is only displayed for the nAChR; for GLIC, the two averaged values were 155 ms and 169 ms. All current traces shown in this figure are the averages of 10–25 consecutive responses recorded from representative patches.

work on their animal—both vertebrate and invertebrate—counterparts. Indeed, the differences identified between the bacterial and animal pLGICs were not much larger than those found between distantly related pLGICs from animals. For example, although the notion that GLIC is gated by an unusual agonist may have seemed surprising, it was already known that roundworms, mites, flies, and polychaete worms also have proton-gated pLGICs (Schnizler et al., 2005; Mounsey et al., 2007; Beg et al., 2008; Juneja et al., 2014), and that humans, dogs and cows have Zn^{2+}-gated pLGICs (Davies et al., 2003; Houtani et al., 2005). Also, although the slow activation of ELIC upon fast exposure to a saturating concentration of a high-efficacy agonist (time constant = 38 ± 6 ms for 50 mM cysteamine in outside-out patches excised from HEK-293 cells; 7 patches) may have seemed uncharacteristic, it was well-known that the mouse serotonin type-3A receptor (5-HT_{3A}R) also activates with a time course that is uncharacteristically slow for a neurotransmitter-gated channel (time constant ≅ 7.3 ms in outside-out patches excised from HEK-293 cells; Mott et al., 2001). Moreover, although the presence of a ring of five pore-occluding phenylalanines may have seemed a unique property of ELIC, examination of invertebrate genomes had revealed the existence of several pLGIC subunits from roundworms, sea squirts, and sea anemones that also contain a phenylalanine at position 16′ of the transmembrane M2 α-helix and that may also assemble as homopentamers in vivo (Beg and Jorgensen, 2003; Satoh et al., 2006; Putnam et al., 2007; Rufener et al., 2009). Furthermore, nothing seemed particularly remarkable about the single-channel conductance values of GLIC and ELIC. Indeed, GLIC's value (∼8 pS; Bocquet et al., 2007) is similar to that of the 5-HT_{3A}R–5-HT_{3B}R heteromer (∼16 pS; Davies et al., 1999), whereas ELIC's (∼84 pS; Zimmermann and Dutzler, 2011) is nearly the same as that of the adult-muscle nAChR (∼73 pS; Elenes et al.,

TABLE 4

Effect of mutations at position 9′ of the M2 α-helix on the time course of deactivation

Channel	$\tau_{deactivation}$		P-value	Number of patches
	(mean ± SE; ms)	(range; ms)		
Wild-type nAChR	1.12 ± 0.10	0.77–1.71	1.0×10^{-15}	12
αL9′A AChR	100 ± 5	88.9–112		4
Wild-type GLIC	0.91 ± 0.20	0.41–1.91	–	11
I9′A GLIC[a]	162	155; 169		2
Wild-type ELIC	17.2 ± 3.2	7.34–26.3	–	6
L9′A ELIC	5.01 ± 0.95	4.02–9.23	2.7×10^{-3}	6
L9′A + F16′L ELIC	5.11 ± 1.04	4.01–9.61	3.0×10^{-3}	6
L9′Q ELIC	15.3 ± 1.9	8.75–18.4	0.60	6
L9′E ELIC	12.6 ± 0.9	10.4–15.3	0.17	6

[a]High-quality recordings could only be obtained from two outside-out patches. Hence, neither the standard error nor the p-value was calculated.

2009) for inward currents recorded under comparable ion conditions.

In contrast, here, we presented experimental evidence for the notion that the superfamily of nicotinic receptor-like channels is functionally more diverse than previously thought. We found that ELIC displays a remarkably atypical response to several perturbations that have long been used to probe the pLGICs from animals. Specifically, ELIC is not blocked by quaternary-ammonium cations TMA^+ or TEA^+ applied extracellularly at a concentration as high as 50 mM; displays a slower macroscopic current-decay time course in the presence of lidocaine and a saturating concentration of agonist; binds lidocaine in the cavities delimited by the M1, M2, and M3 transmembrane α-helices; and deactivates with wild-type-like kinetics—or even faster—upon the introduction of mutations that reduce the hydrophobicity of the channel's transmembrane pore lining. Instead, all other cation-selective pLGICs studied to date are blocked by extracellular TMA^+ and TEA^+ in the micromolar-to-millimolar concentration range (Adler et al., 1979; Marshall et al., 1990; Zhang et al., 1995; Blanchet and Dulon, 2001; Akk and Steinbach, 2003), their current-decay time course in the presence of a saturating concentration of agonist becomes faster upon lidocaine binding (Alberola-Die et al., 2011) to the M2-delimited pore cavity (Hilf et al., 2010), and deactivate much more slowly upon engineering mutations such as those tested here (Filatov and White, 1995; Labarca et al., 1995; Kosolapov et al., 2000; Papke and Grosman, 2014).

Thompson et al. (2012) reported that TMA^+ and TEA^+ at a concentration of ∼20 mM reduce the peak-amplitude of currents mediated by ELIC by a factor of ∼2, a result that may seem to contradict our findings presented above. However, it should be noted that, in these experiments, ELIC currents were elicited by 1.6 mM GABA, a concentration of agonist that elicits only a half-maximal response (EC_{50}). In contrast, in our experiments, ELIC currents were elicited by a saturating concentration of cysteamine. Thus, we surmise that the reported inhibitory effect of TMA^+ and TEA^+ reflects the competition of these quaternary-ammonium cations (which, when applied alone, do not elicit any measurable current response; Thompson et al. [2012]) with GABA for the channel's agonist-binding sites rather than the blocking of the pore. Indeed, it has been reported that TMA^+ competes with cysteamine (Zimmermann et al., 2012) for the agonist-binding sites of ELIC, but their relative affinities are such that, at a concentration of cysteamine as high as 10 mM (i.e., the value we used in our experiments), TMA^+ is expected to be outcompeted even when present at a concentration of 50 mM. Therefore, there is no discrepancy between our results and those reported by Thompson et al. (2012).

No discrete feature of the amino-acid sequence of ELIC seemed "suspicious" to us so as to anticipate its unique pore properties, and thus, it seems impossible to predict ELIC-like behavior in newly discovered pLGIC subunits on the basis of sequence gazing alone. Furthermore, because only a structural model for a nonconductive conformation of ELIC is currently available (Hilf and Dutzler, 2008), identifying the three-dimensional structural basis for its unusual open-channel behavior does not seem straightforward, either. Perhaps, however, the lack of block by 50 mM TMA^+ or TEA^+ would be the simplest property to explain if the most intracellular turn of each of the five M2 α-helices moved little upon opening (relative to their position in the nonconductive crystallized conformation) and formed the narrowest constriction in the open-channel conformation. Indeed, the diameter of the pore at the level of the intracellular ends of the M2 α-helices in the crystallized

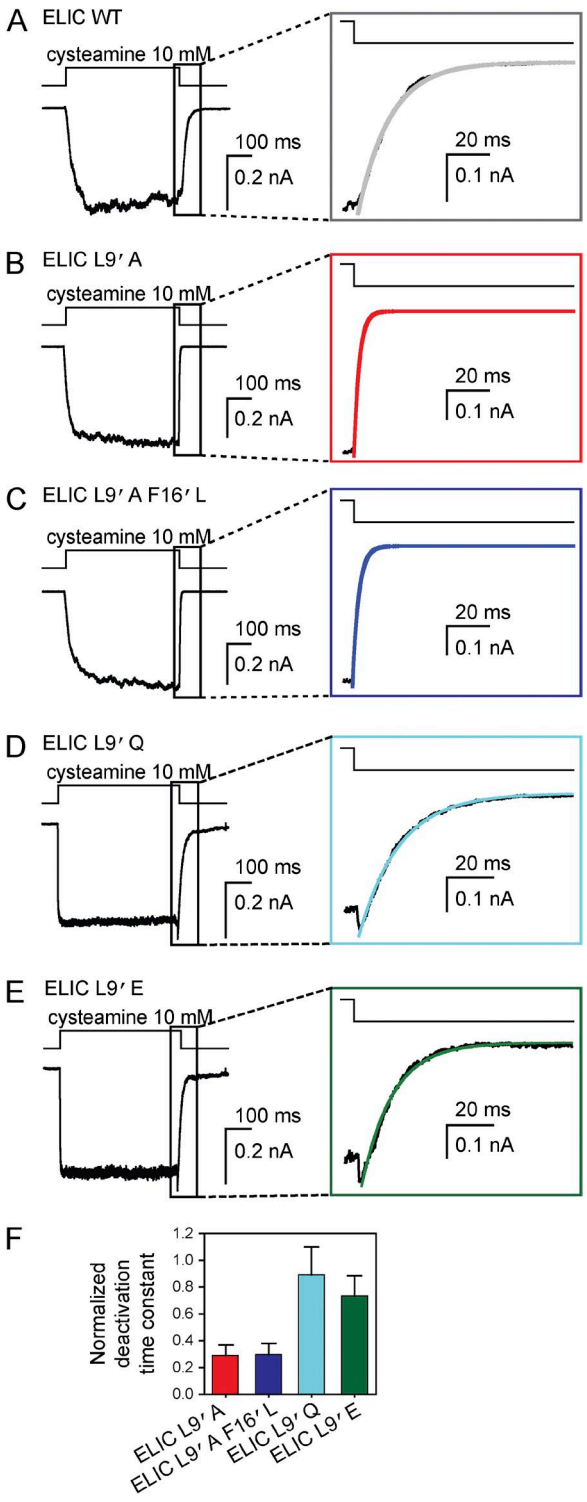

Figure 16. Effect of mutations at position 9′ of M2 on deactivation of ELIC. (A–E) Macroscopic current responses to 500-ms pulses of 10 mM cysteamine recorded at –80 mV from wild-type ELIC and the indicated mutants in the outside-out configuration. The solutions flowing through the two barrels of the perfusion tubing were (in mM) 142 KCl, 5.4 NaCl, 1.8 $CaCl_2$, 1.7 $MgCl_2$, and 10 HEPES/KOH, pH 7.4 with or without cysteamine. The insets emphasize the time courses of deactivation; lines are fits to monoexponential-decay functions. (F) Mutant-construct deactivation time constants obtained from monoexponential fits normalized to the wild-type time constant. The plotted values are means obtained from 6 patches for each mutant; error bars are the corresponding standard errors. All current traces shown in this figure are the averages of 10 consecutive responses recorded from representative patches.

nonconductive conformation of ELIC is ∼9 Å, a size that would be consistent with the relatively high permeation rate observed for TMA^+, TEA^+, and TPA^+. For comparison, in a homology model of the open-channel conformation of the mouse muscle nAChR, this diameter is ∼7 Å (Harpole and Grosman, 2014), whereas in the open-channel model of GLIC (Protein Data Bank ID code 4HFI; Sauguet et al., 2013), it is 5.2 Å (forcing the side chains of the five pore-lining glutamates at position –2′ to move out of the way by adopting a rotamer with $\chi_1 \cong -60°$ and $\chi_2 \cong +60°$; otherwise, the diameter would be even narrower). It is tempting to speculate that it is this putatively larger size of the transmembrane pore cavity in the open state of ELIC that also underlies the lower binding affinity for TMA^+ and TEA^+, and the atypical effect of mutations to pore-lining residues on the kinetics of deactivation.

The physiological role of ELIC in the bacterium *Erwinia chrysanthemi* (now reclassified as *Dickeya dadantii*) is not known. However, we reason that the low affinity of ELIC for quaternary-ammonium cations, for example, would be advantageous if the channel faced an external solution that is rich in hydrophobic cations, and yet, the bacterium required a fast influx of inorganic cations—such as Na^+ and Ca^{2+}—through the channel's cation-selective pore. In addition, it is likely that permeant organic cations for which the pore of ELIC has a higher affinity (higher than for TMA^+, TEA^+ or TPA^+) exist. If this were the case, and if such cations indeed existed in the solutions bathing the bacterial membrane, then ELIC could function as a channel for solutes other than small inorganic cations. Clearly, extensive future work will be required to elucidate how the peculiar properties of this channel give rise to its biological function. Moreover, there may well be other pLGICs that behave like ELIC among the largely unexplored bacterial, archaeal, and invertebrate members of the superfamily, and thus, ELIC's unconventional features may turn out to be less unusual than we currently think.

As for its role as a model system for the entire superfamily, our data indicate that caution should be exercised when generalizing results obtained with ELIC to the rest of the pLGICs, especially as they pertain to the properties of the transmembrane pore domain. Nevertheless, we would like to emphasize the notion that a member with such different functional properties in the context of a well-conserved three-dimensional architecture offers an unparalleled opportunity to further

our mechanistic understanding of the pLGICs from vertebrate animals.

We thank Keith Brister, Joseph Brunzelle, David Smith, Elena Kondrashkina, Spencer Anderson, and Zdzislaw Wawrzak (Life Sciences Collaborative Access Team, 21 ID–D/F/G at Argonne National Laboratory, Advanced Photon Source) for technical assistance during crystallographic data collection; S. Sine (Mayo Clinic, Rochester, MN) for wild-type muscle nAChR subunit cDNAs; Y. Bello, C. Johnson, N. Kowalczyk, M. Rigby, and G. Wang for assistance with mutagenesis, cell culturing and transfections; and T. Harpole for the critical reading of the manuscript.

This work was supported by National Institutes of Health Grant NS042169 (to C. Grosman) and the Richard and Margaret Romano Professorial Scholarship (to C. Grosman).

The authors declare no competing financial interests.

Sharona E. Gordon served as editor.

Submitted: 25 November 2014
Accepted: 14 May 2015

REFERENCES

Adams, D.J., T.M. Dwyer, and B. Hille. 1980. The permeability of endplate channels to monovalent and divalent metal cations. *J. Gen. Physiol.* 75:493–510.

Adams, P.D., P.V. Afonine, G. Bunkóczi, V.B. Chen, I.W. Davis, N. Echols, J.J. Headd, L.-W. Hung, G.J. Kapral, R.W. Grosse-Kunstleve, et al. 2010. PHENIX: a comprehensive Python-based system for macromolecular structure solution. *Acta Crystallogr. D Biol. Crystallogr.* 66:213–221. http://dx.doi.org/10.1107/S0907444909052925

Adler, M., A.C. Oliveira, E.X. Albuquerque, N.A. Mansour, and A.T. Eldefrawi. 1979. Reaction of tetraethylammonium with the open and closed conformations of the acetylcholine receptor ionic channel complex. *J. Gen. Physiol.* 74:129–152. http://dx.doi.org/10.1085/jgp.74.1.129

Akk, G., and J.H. Steinbach. 2003. Activation and block of mouse muscle-type nicotinic receptors by tetraethylammonium. *J. Physiol.* 551:155–168. http://dx.doi.org/10.1113/jphysiol.2003.043885

Alberola-Die, A., J. Martinez-Pinna, J.M. González-Ros, I. Ivorra, and A. Morales. 2011. Multiple inhibitory actions of lidocaine on *Torpedo* nicotinic acetylcholine receptors transplanted to *Xenopus* oocytes. *J. Neurochem.* 117:1009–1019.

Avdeef, A., and J.A. Brown. 1984. Calcium binding by biological ligands. 2 [1]. Formation of protonated and polynuclear complexes between cadmium and 2-mercaptoethylamine. *Inorg. Chim. Acta.* 91:67–73.

Bali, M., and M.H. Akabas. 2007. The location of a closed channel gate in the $GABA_A$ receptor channel. *J. Gen. Physiol.* 129:145–159. http://dx.doi.org/10.1085/jgp.200609639

Beg, A.A., and E.M. Jorgensen. 2003. EXP-1 is an excitatory GABA-gated cation channel. *Nat. Neurosci.* 6:1145–1152. http://dx.doi.org/10.1038/nn1136

Beg, A.A., G.G. Ernstrom, P. Nix, M.W. Davis, and E.M. Jorgensen. 2008. Protons act as a transmitter for muscle contraction in *C. elegans*. *Cell.* 132:149–160. http://dx.doi.org/10.1016/j.cell.2007.10.058

Bianchi, M.T., and R.L. Macdonald. 2001. Mutation of the 9′ leucine in the GABA(A) receptor γ2L subunit produces an apparent decrease in desensitization by stabilizing open states without altering desensitized states. *Neuropharmacology.* 41:737–744. http://dx.doi.org/10.1016/S0028-3908(01)00132-0

Blanchet, C., and D. Dulon. 2001. Tetraethylammonium ions block the nicotinic cholinergic receptors of cochlear outer hair cells. *Brain Res.* 915:11–17. http://dx.doi.org/10.1016/S0006-8993(01)02806-2

Bocquet, N., L. Prado de Carvalho, J. Cartaud, J. Neyton, C. Le Poupon, A. Taly, T. Grutter, J.-P. Changeux, and P.-J. Corringer. 2007. A prokaryotic proton-gated ion channel from the nicotinic acetylcholine receptor family. *Nature.* 445:116–119. http://dx.doi.org/10.1038/nature05371

Burzomato, V., P.J. Groot-Kormelink, L.G. Sivilotti, and M. Beato. 2003. Stoichiometry of recombinant heteromeric glycine receptors revealed by a pore-lining region point mutation. *Receptors Channels.* 9:353–361.

Chang, Y., and D.S. Weiss. 1998. Substitutions of the highly conserved M2 leucine create spontaneously opening rho1 gamma-aminobutyric acid receptors. *Mol. Pharmacol.* 53:511–523.

Chang, Y., and D.S. Weiss. 1999. Allosteric activation mechanism of the alpha 1 beta 2 gamma 2 gamma-aminobutyric acid type A receptor revealed by mutation of the conserved M2 leucine. *Biophys. J.* 77:2542–2551. http://dx.doi.org/10.1016/S0006-3495(99)77089-X

Charnet, P., C. Labarca, R.J. Leonard, N.J. Vogelaar, L. Czyzyk, A. Gouin, N. Davidson, and H.A. Lester. 1990. An open-channel blocker interacts with adjacent turns of α-helices in the nicotinic acetylcholine receptor. *Neuron.* 4:87–95. http://dx.doi.org/10.1016/0896-6273(90)90445-L

Chen, J., Y. Zhang, G. Akk, S. Sine, and A. Auerbach. 1995. Activation kinetics of recombinant mouse nicotinic acetylcholine receptors: mutations of α-subunit tyrosine 190 affect both binding and gating. *Biophys. J.* 69:849–859. http://dx.doi.org/10.1016/S0006-3495(95)79959-3

Conway, B.E., R.E. Verrall, and J.E. Desnoyers. 1966. Partial molal volumes of tetraalkylammonium halides and assignment of individual ionic contributions. *Trans. Faraday Soc.* 62:2738–2749. http://dx.doi.org/10.1039/tf9666202738

Cuevas, J., and D.J. Adams. 1994. Local anaesthetic blockade of neuronal nicotinic ACh receptor-channels in rat parasympathetic ganglion cells. *Br. J. Pharmacol.* 111:663–672.

Cymes, G.D., C. Grosman, and A. Auerbach. 2002. Structure of the transition state of gating in the acetylcholine receptor channel pore: a phi-value analysis. *Biochemistry.* 41:5548–5555. http://dx.doi.org/10.1021/bi011864f

Cymes, G.D., Y. Ni, and C. Grosman. 2005. Probing ion-channel pores one proton at a time. *Nature.* 438:975–980. http://dx.doi.org/10.1038/nature04293

Davies, P.A., M. Pistis, M.C. Hanna, J.A. Peters, J.J. Lambert, T.G. Hales, and E.F. Kirkness. 1999. The $5\text{-}HT_{3B}$ subunit is a major determinant of serotonin-receptor function. *Nature.* 397:359–363. http://dx.doi.org/10.1038/16941

Davies, P.A., W. Wang, T.G. Hales, and E.F. Kirkness. 2003. A novel class of ligand-gated ion channel is activated by Zn^{2+}. *J. Biol. Chem.* 278:712–717.

Decker, E.R., and J.A. Dani. 1990. Calcium permeability of the nicotinic acetylcholine receptor: the single-channel calcium influx is significant. *J. Neurosci.* 10:3413–3420.

Edward, J.T. 1970. Molecular volumes and the Stokes-Einstein equation. *J. Chem. Educ.* 47:261–270. http://dx.doi.org/10.1021/ed047p261

Elenes, S., Y. Ni, G.D. Cymes, and C. Grosman. 2006. Desensitization contributes to the synaptic response of gain-of-function mutants of the muscle nicotinic receptor. *J. Gen. Physiol.* 128:615–627.

Elenes, S., M. Decker, G.D. Cymes, and C. Grosman. 2009. Decremental response to high-frequency trains of acetylcholine pulses but unaltered fractional Ca^{2+} currents in a panel of "slow-channel syndrome" nicotinic receptor mutants. *J. Gen. Physiol.* 133:151–169. http://dx.doi.org/10.1085/jgp.200810089

Emsley, P., B. Lohkamp, W.G. Scott, and K. Cowtan. 2010. Features and development of Coot. *Acta Crystallogr. D Biol. Crystallogr.* 66:486–501. http://dx.doi.org/10.1107/S0907444910007493

Etter, A., D.F. Cully, K.K. Liu, B. Reiss, D.K. Vassilatis, J.M. Schaeffer, and J.P. Arena. 1999. Picrotoxin blockade of invertebrate glutamate-gated chloride channels: subunit dependence and evidence for binding within the pore. *J. Neurochem.* 72:318–326.

Filatov, G.N., and M.M. White. 1995. The role of conserved leucines in the M2 domain of the acetylcholine receptor in channel gating. *Mol. Pharmacol.* 48:379–384.

Gonzalez-Gutierrez, G., and C. Grosman. 2010. Bridging the gap between structural models of nicotinic receptor superfamily ion channels and their corresponding functional states. *J. Mol. Biol.* 403:693–705.

Gonzalez-Gutierrez, G., T. Lukk, V. Agarwal, D. Papke, S.K. Nair, and C. Grosman. 2012. Mutations that stabilize the open state of the *Erwinia chrisanthemi* ligand-gated ion channel fail to change the conformation of the pore domain in crystals. *Proc. Natl. Acad. Sci. USA.* 109:6331–6336. http://dx.doi.org/10.1073/pnas.1119268109

Gonzalez-Gutierrez, G., L.G. Cuello, S.K. Nair, and C. Grosman. 2013. Gating of the proton-gated ion channel from *Gloeobacter violaceus* at pH 4 as revealed by X-ray crystallography. *Proc. Natl. Acad. Sci. USA.* 110:18716–18721.

Grosman, C. 2003. Free-energy landscapes of ion-channel gating are malleable: changes in the number of bound ligands are accompanied by changes in the location of the transition state in acetylcholine-receptor channels. *Biochemistry.* 42:14977–14987. http://dx.doi.org/10.1021/bi0354334

Hansen, S.B., G. Sulzenbacher, T. Huxford, P. Marchot, P. Taylor, and Y. Bourne. 2005. Structures of *Aplysia* AChBP complexes with nicotinic agonists and antagonists reveal distinctive binding interfaces and conformations. *EMBO J.* 24:3635–3646.

Harpole, T.J., and C. Grosman. 2014. Side-chain conformation at the selectivity filter shapes the permeation free-energy landscape of an ion channel. *Proc. Natl. Acad. Sci. USA.* 111:E3196–E3205. http://dx.doi.org/10.1073/pnas.1408950111

Hibbs, R.E., and E. Gouaux. 2011. Principles of activation and permeation in an anion-selective Cys-loop receptor. *Nature.* 474:54–60. http://dx.doi.org/10.1038/nature10139

Hilf, R.J.C., and R. Dutzler. 2008. X-ray structure of a prokaryotic pentameric ligand-gated ion channel. *Nature.* 452:375–379. http://dx.doi.org/10.1038/nature06717

Hilf, R.J.C., C. Bertozzi, I. Zimmermann, A. Reiter, D. Trauner, and R. Dutzler. 2010. Structural basis of open channel block in a prokaryotic pentameric ligand-gated ion channel. *Nat. Struct. Mol. Biol.* 17:1330–1336. http://dx.doi.org/10.1038/nsmb.1933

Houtani, T., Y. Munemoto, M. Kase, S. Sakuma, T. Tsutsumi, and T. Sugimoto. 2005. Cloning and expression of ligand-gated ion-channel receptor L2 in central nervous system. *Biochem. Biophys. Res. Commun.* 335:277–285.

Jones, M.V., and G.L. Westbrook. 1995. Desensitized states prolong $GABA_A$ channel responses to brief agonist pulses. *Neuron.* 15:181–191. http://dx.doi.org/10.1016/0896-6273(95)90075-6

Juneja, P., R. Horlacher, D. Bertrand, R. Krause, F. Marger, and W. Welte. 2014. An internally modulated, thermostable, pH-sensitive Cys loop receptor from the hydrothermal vent worm *Alvinella pompejana*. *J. Biol. Chem.* 289:15130–15140.

Kearney, P.C., H. Zhang, W. Zhong, D.A. Dougherty, and H.A. Lester. 1996. Determinants of nicotinic receptor gating in natural and unnatural side chain structures at the M2 9′ position. *Neuron.* 17:1221–1229. http://dx.doi.org/10.1016/S0896-6273(00)80252-4

Kosolapov, A.V., G.N. Filatov, and M.M. White. 2000. Acetylcholine receptor gating is influenced by the polarity of amino acids at position 9′ in the M2 domain. *J. Membr. Biol.* 174:191–197. http://dx.doi.org/10.1007/s002320001043

Labarca, C., M.W. Nowak, H. Zhang, L. Tang, P. Deshpande, and H.A. Lester. 1995. Channel gating governed symmetrically by conserved leucine residues in the M2 domain of nicotinic receptors. *Nature.* 376:514–516. http://dx.doi.org/10.1038/376514a0

Leonard, R.J., C.G. Labarca, P. Charnet, N. Davidson, and H.A. Lester. 1988. Evidence that the M2 membrane-spanning region lines the ion channel pore of the nicotinic receptor. *Science.* 242:1578–1581. http://dx.doi.org/10.1126/science.2462281

Marabelli, A., R. Lape, and L. Sivilotti. 2015. Mechanism of activation of the prokaryotic channel ELIC by propylamine: a single-channel study. *J. Gen. Physiol.* 145:23–45. http://dx.doi.org/10.1085/jgp.201411234

Marshall, J., S.D. Buckingham, R. Shingai, G.G. Lunt, M.W. Goosey, M.G. Darlison, D.B. Sattelle, and E.A. Barnard. 1990. Sequence and functional expression of a single α subunit of an insect nicotinic acetylcholine receptor. *EMBO J.* 9:4391–4398.

Mott, D.D., K. Erreger, T.G. Banke, and S.F. Traynelis. 2001. Open probability of homomeric murine $5\text{-}HT_{3A}$ serotonin receptors depends on subunit occupancy. *J. Physiol.* 535:427–443.

Mounsey, K.E., J.A. Dent, D.C. Holt, J. McCarthy, B.J. Currie, and S.F. Walton. 2007. Molecular characterisation of a pH-gated chloride channel from *Sarcoptes scabiei*. *Invert. Neurosci.* 7:149–156.

Mukhtasimova, N., W.Y. Lee, H.-L. Wang, and S.M. Sine. 2009. Detection and trapping of intermediate states priming nicotinic receptor channel opening. *Nature.* 459:451–454. http://dx.doi.org/10.1038/nature07923

Neher, E., and J.H. Steinbach. 1978. Local anaesthetics transiently block currents through single acetylcholine-receptor channels. *J. Physiol.* 277:153–176. http://dx.doi.org/10.1113/jphysiol.1978.sp012267

Ogden, D.C., and D. Colquhoun. 1985. Ion channel block by acetylcholine, carbachol and suberyldicholine at the frog neuromuscular junction. *Proc. R. Soc. Lond. B Biol. Sci.* 225:329–355.

Ohno, K., D.O. Hutchinson, M. Milone, J.M. Brengman, C. Bouzat, S.M. Sine, and A.G. Engel. 1995. Congenital myasthenic syndrome caused by prolonged acetylcholine receptor channel openings due to a mutation in the M2 domain of the ε subunit. *Proc. Natl. Acad. Sci. USA.* 92:758–762.

Otwinowski, Z., and W. Minor. 1997. Processing of X-ray Diffraction Data Collected in Oscillation Mode. *In* Methods Enzymol. 276: Macromolecular Crystallography, part A. C.W. Carter, Jr., and R.M. Sweet, editors. Academic Press. 307–326.

Papke, D., and C. Grosman. 2014. The role of intracellular linkers in gating and desensitization of human pentameric ligand-gated ion channels. *J. Neurosci.* 34:7238–7252. http://dx.doi.org/10.1523/JNEUROSCI.5105-13.2014

Parikh, R.B., M. Bali, and M.H. Akabas. 2011. Structure of the M2 transmembrane segment of GLIC, a prokaryotic Cys loop receptor homologue from *Gloeobacter violaceus*, probed by substituted cysteine accessibility. *J. Biol. Chem.* 286:14098–14109. http://dx.doi.org/10.1074/jbc.M111.221895

Purohit, P., and A. Auerbach. 2013. Loop C and the mechanism of acetylcholine receptor-channel gating. *J. Gen. Physiol.* 141:467–478.

Purohit, Y., and C. Grosman. 2006. Block of muscle nicotinic receptors by choline suggests that the activation and desensitization gates act as distinct molecular entities. *J. Gen. Physiol.* 127:703–717. http://dx.doi.org/10.1085/jgp.200509437

Putnam, N.H., M. Srivastava, U. Hellsten, B. Dirks, J. Chapman, A. Salamov, A. Terry, H. Shapiro, E. Lindquist, V.V. Kapitonov, et al. 2007. Sea anemone genome reveals ancestral eumetazoan gene repertoire and genomic organization. *Science.* 317:86–94. http://dx.doi.org/10.1126/science.1139158

Revah, F., D. Bertrand, J.L. Galzi, A. Devillers-Thiéry, C. Mulle, N. Hussy, S. Bertrand, M. Ballivet, and J.P. Changeux. 1991. Mutations in the channel domain alter desensitization of a neuronal nicotinic receptor. *Nature.* 353:846–849. http://dx.doi.org/10.1038/353846a0

Rufener, L., P. Mäser, I. Roditi, and R. Kaminsky. 2009. *Haemonchus contortus* acetylcholine receptors of the DEG-3 subfamily and their role in sensitivity to monepantel. *PLoS Pathog.* 5:e1000380. http://dx.doi.org/10.1371/journal.ppat.1000380

Satoh, N., T. Kawashima, E. Shoguchi, and Y. Satou. 2006. Urochordate genomes. *Genome Dyn.* 2:198–212.

Sauguet, L., F. Poitevin, S. Murail, C. Van Renterghem, G. Moraga-Cid, L. Malherbe, A.W. Thompson, P. Koehl, P.-J. Corringer, M. Baaden, and M. Delarue. 2013. Structural basis for ion permeation mechanism in pentameric ligand-gated ion channels. *EMBO J.* 32:728–741. http://dx.doi.org/10.1038/emboj.2013.17

Schnizler, K., B. Saeger, C. Pfeffer, A. Gerbaulet, U. Ebbinghaus-Kintscher, C. Methfessel, E.-M. Franken, K. Raming, C.H. Wetzel, A. Saras, et al. 2005. A novel chloride channel in *Drosophila melanogaster* is inhibited by protons. *J. Biol. Chem.* 280:16254–16262.

Sedelnikova, A., B.E. Erkkila, H. Harris, S.O. Zakharkin, and D.S. Weiss. 2006. Stoichiometry of a pore mutation that abolishes picrotoxin-mediated antagonism of the $GABA_A$ receptor. *J. Physiol.* 577:569–577.

Shan, Q., S.T. Nevin, J.L. Haddrill, and J.W. Lynch. 2003. Asymmetric contribution of α and β subunits to the activation of αβ heteromeric glycine receptors. *J. Neurochem.* 86:498–507. http://dx.doi.org/10.1046/j.1471-4159.2003.01872.x

Shen, X.-M., J.M. Brengman, S.M. Sine, and A.G. Engel. 2012. Myasthenic syndrome AChRα C-loop mutant disrupts initiation of channel gating. *J. Clin. Invest.* 122:2613–2621. http://dx.doi.org/10.1172/JCI63415

Sine, S.M., and J.H. Steinbach. 1984. Agonists block currents through acetylcholine receptor channels. *Biophys. J.* 46:277–283. http://dx.doi.org/10.1016/S0006-3495(84)84022-9

Tasneem, A., L.M. Iyer, E. Jakobsson, and L. Aravind. 2005. Identification of the prokaryotic ligand-gated ion channels and their implications for the mechanisms and origins of animal Cys-loop ion channels. *Genome Biol.* 6:R4. http://dx.doi.org/10.1186/gb-2004-6-1-r4

Thompson, S.A., M.Z. Smith, P.B. Wingrove, P.J. Whiting, and K.A. Wafford. 1999. Mutation at the putative $GABA_A$ ion-channel gate reveals changes in allosteric modulation. *Br. J. Pharmacol.* 127:1349–1358. http://dx.doi.org/10.1038/sj.bjp.0702687

Thompson, A.J., M. Alqazzaz, C. Ulens, and S.C.R. Lummis. 2012. The pharmacological profile of ELIC, a prokaryotic GABA-gated receptor. *Neuropharmacology.* 63:761–767. http://dx.doi.org/10.1016/j.neuropharm.2012.05.027

Ue, M. 1994. Mobility and ionic association of lithium and quaternary ammonium salts in propylene carbonate and γ-butyrolactone. *J. Electrochem. Soc.* 141:3336–3342. http://dx.doi.org/10.1149/1.2059336

Velisetty, P., and S. Chakrapani. 2012. Desensitization mechanism in prokaryotic ligand-gated ion channel. *J. Biol. Chem.* 287:18467–18477. http://dx.doi.org/10.1074/jbc.M112.348045

Wang, D.-S., R. Buckinx, H. Lecorronc, J.-M. Mangin, J.-M. Rigo, and P. Legendre. 2007. Mechanisms for picrotoxinin and picrotin blocks of α_2 homomeric glycine receptors. *J. Biol. Chem.* 282:16016–16035. http://dx.doi.org/10.1074/jbc.M701502200

Wyllie, D.J., P. Béhé, and D. Colquhoun. 1998. Single-channel activations and concentration jumps: comparison of recombinant NR1a/NR2A and NR1a/NR2D NMDA receptors. *J. Physiol.* 510:1–18.

Yang, J. 1990. Ion permeation through 5-hydroxytryptamine-gated channels in neuroblastoma N18 cells. *J. Gen. Physiol.* 96:1177–1198. http://dx.doi.org/10.1085/jgp.96.6.1177

Yoluk, O., T. Brömstrup, E.J. Bertaccini, J.R. Trudell, and E. Lindahl. 2013. Stabilization of the GluCl ligand-gated ion channel in the presence and absence of ivermectin. *Biophys. J.* 105:640–647. http://dx.doi.org/10.1016/j.bpj.2013.06.037

Zhang, Y., J. Chen, and A. Auerbach. 1995. Activation of recombinant mouse acetylcholine receptors by acetylcholine, carbamylcholine and tetramethylammonium. *J. Physiol.* 486:189–206. http://dx.doi.org/10.1113/jphysiol.1995.sp020802

Zhou, Z., and E. Neher. 1993. Calcium permeability of nicotinic acetylcholine receptor channels in bovine adrenal chromaffin cells. *Pflugers Arch.* 425:511–517. http://dx.doi.org/10.1007/BF00374879

Zimmermann, I., and R. Dutzler. 2011. Ligand activation of the prokaryotic pentameric ligand-gated ion channel ELIC. *PLoS Biol.* 9:e1001101. http://dx.doi.org/10.1371/journal.pbio.1001101

Zimmermann, I., A. Marabelli, C. Bertozzi, L.G. Sivilotti, and R. Dutzler. 2012. Inhibition of the prokaryotic pentameric ligand-gated ion channel ELIC by divalent cations. *PLoS Biol.* 10:e1001429. http://dx.doi.org/10.1371/journal.pbio.1001429